iScience

CellPress
OPEN ACCESS

Article

Group 2 Innate Lymphoid Cells Exacerbate Amebic Liver Abscess in Mice

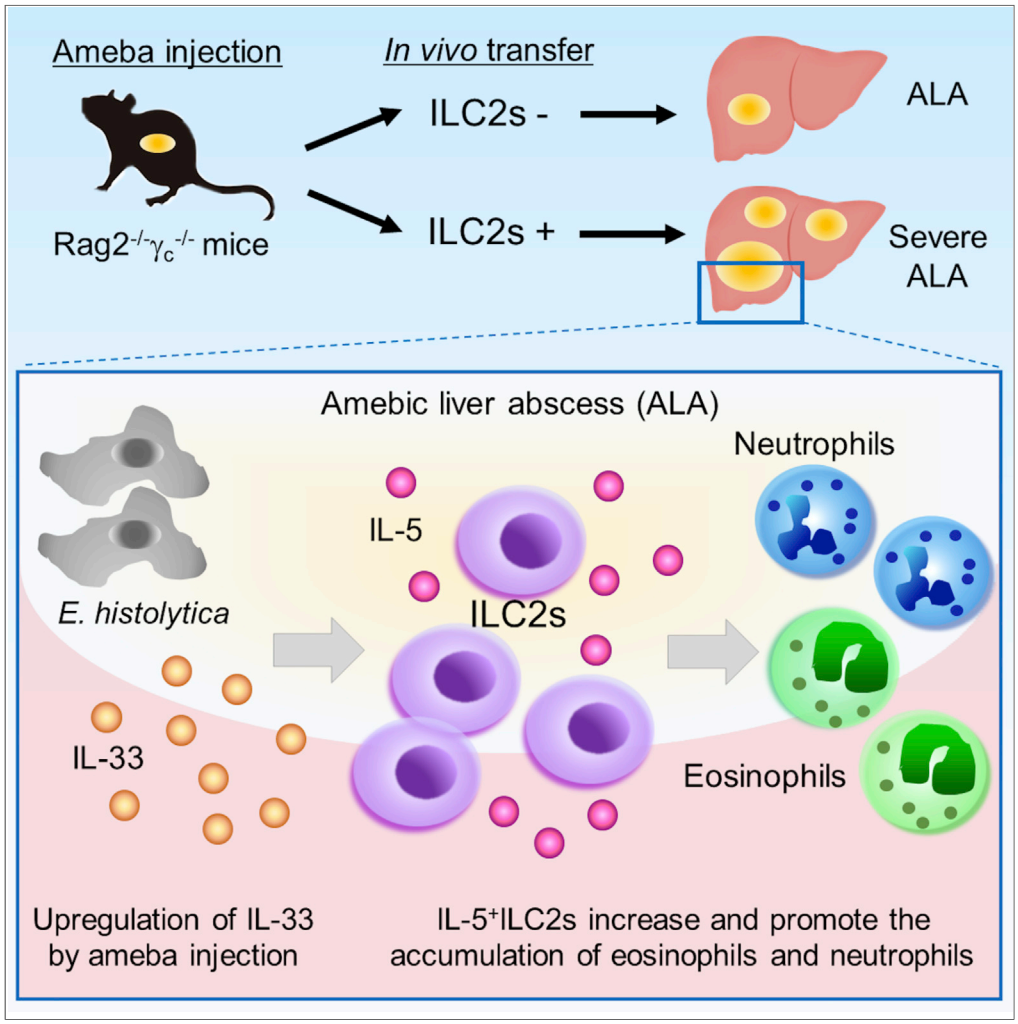

Risa Nakamura, Akihiro Yoshizawa, Taeko Moriyasu, ..., Shigeo Koyasu, Kazuyo Moro, Shinjiro Hamano

risa-n@nagasaki-u.ac.jp (R.N.)
shinjiro@nagasaki-u.ac.jp (S.H.)

HIGHLIGHTS

ILC2s exacerbate ALA by promoting the accumulation of eosinophils and neutrophils

Hepatic ILC2s are increased and the main source of IL-5 in the early phase of ALA

Hepatic ILC2s localize with IL-33^{+} cells in the inflammatory areas of ALA

IL-33 is a trigger of ILC2-mediated ALA formation

Nakamura et al., iScience *23*, 101544
September 25, 2020
https://doi.org/10.1016/j.isci.2020.101544

iScience

CellPress
OPEN ACCESS

Article

Group 2 Innate Lymphoid Cells Exacerbate Amebic Liver Abscess in Mice

Risa Nakamura,[1,2,3,*] Akihiro Yoshizawa,[4,5] Taeko Moriyasu,[2,3,6] Sharmina Deloer,[1,2,3,7] Masachika Senba,[3,8] Mihoko Kikuchi,[3,9] Shigeo Koyasu,[10,11] Kazuyo Moro,[4,12] and Shinjiro Hamano[1,2,3,13,*]

SUMMARY

***Entamoeba histolytica*, a protozoan parasite in the lumen of the human large intestine, occasionally spreads to the liver and induces amebic liver abscesses (ALAs). Upon infection with *E. histolytica*, high levels of type 2 cytokines are induced in the liver early after infection. However, the sources and functions of these initial type 2 cytokines in ALA formation remain unclear. In this study, we examined the roles of group 2 innate lymphoid cells (ILC2s) in ALA formation. Hepatic ILC2 numbers were significantly increased and they produced robust levels of IL-5. The *in vivo* transfer of ILC2s into Rag2$^{-/-}$common γ chain (γ_c)$^{-/-}$ KO mice aggravated ALA formation accompanied by eosinophilia and neutrophilia. Furthermore, IL-33-deficient mice and IL-5-neutralized mice had less ALA formations. These results suggest that ILC2s contribute to exacerbating the pathogenesis of ALA by producing early type 2 cytokines and promoting the accumulation of eosinophils and neutrophils in the liver.**

INTRODUCTION

In developing countries where the social infrastructure and hygienic environment are poor, pathogenic parasites often contaminate water and food and cause intestinal infectious diseases in humans. Amebiasis is caused by infection with *Entamoeba histolytica*, an enteric protozoan parasite, and it remains as a leading parasitic disease globally, affecting about 50 million people and causing 55,500 deaths each year (Kotloff et al., 2013; Murray et al., 2012). Occasionally, *E. histolytica* invades the intestinal mucosa causing amebic colitis and then spreads to extra-intestinal organs, especially the liver through the portal circulation, resulting in amebic liver abscess (ALA) formation (Hamano et al., 2013; Haque et al., 2003; Ravdin, 1988). Approximately 80% of patients with ALA develop symptoms within 2–4 weeks including fever and abdominal pain, which, if not treated adequately, can cause the progressive focal destruction of liver tissues (Prakash and Bhimji, 2017). However, the factors associated with severe and chronic ALA are unknown.

IFN-γ was critically important in controlling the early formation of ALA in a mouse model of ALA induced by the injection of *E. histolytica* via the liver parenchyma (Lotter et al., 2006; Seydel et al., 2000). *In vitro* studies demonstrated that neutrophils and macrophages, including Kupffer cells, were activated to kill *E. histolytica* by an IFN-γ-dependent mechanism in humans and mice (Denis and Chadee, 1989a, 1989b; Ghadirian and Salimi, 1993; Salata et al., 1987). Thus, IFN-γ activates innate immune cells and prevents severe ALA formation early after *E. histolytica* translocation and invasion.

It is generally accepted that type 1 responses characterized by IFN-γ-dependent mechanism are counteracted by type 2 responses. Type 2 immune responses (IL-4, IL-5, and IL-13) were induced simultaneously with IFN-γ in a mouse model of amebic colitis (Houpt et al., 2002). A hamster model of ALA produced IL-5 and IL-13 at the early phase after the direct injection of *E. histolytica* into the hepatic parenchyma (Cervantes-Rebolledo et al., 2009). Thus far, the source of IL-5 and IL-13 and their roles in ALA formation remain unclear.

Group 2 innate lymphoid cells (ILC2s), a new subset of innate immune cells, produce abundant levels of type 2 cytokines including IL-5, IL-13, and IL-9 in response to epithelial stress signals such as IL-25, IL-33, and thymic stromal lymphopoietin (TSLP). Large amounts of type 2 cytokines secreted by ILC2s are

[1]Department of Parasitology, Institute of Tropical Medicine (NEKKEN), Nagasaki University, Nagasaki, Japan

[2]Graduate School of Biomedical Sciences Doctoral Leadership Program, Nagasaki University, Nagasaki, Japan

[3]The Joint Usage/Research Center on Tropical Disease, Institute of Tropical Medicine (NEKKEN), Nagasaki University, Japan

[4]Laboratory for Innate Immune Systems, RIKEN Center for Integrative Medical Sciences (IMS), Yokohama, Japan

[5]Department of Cardiovascular Medicine, International University of Health and Welfare (IUHW), School of Medicine, Chiba, Japan

[6]Kenya Research Station, Institute of Tropical Medicine (NEKKEN), Nagasaki University, Nagasaki, Japan

[7]Mucosal Immunity Section, Laboratory of Clinical Immunology and Microbiology (LCIM), National Institute of Allergy and infectious Diseases (NIAID), NIH, Maryland, USA

[8]Department of Pathology, Institute of Tropical Medicine (NEKKEN), Nagasaki University, Nagasaki, Japan

[9]Department of Immunogenetics, Institute of Tropical Medicine (NEKKEN), Nagasaki University, Nagasaki, Japan

[10]Laboratory for Immune Cell Systems, RIKEN Center for Integrative Medical Sciences (IMS), Yokohama, Japan

[11]Department of Microbiology and Immunology, Keio University School of Medicine, Tokyo, Japan

Continued

responsible for the initiation of type 2 immune responses. Furthermore, ILC2s had a critical role in the progress of allergic lung inflammation (Halim et al., 2012; Motomura et al., 2014) and the rapid expulsion of intestinal helminths (Moro et al., 2010; Neill et al., 2010). IL-5 secreted by ILC2s induces eosinophil accumulation, and IL-13 upregulates mucin production into the gut to expel enteric nematodes such as *Nippostrongylus brasiliensis*. However, it is unclear whether ILC2s and its production of type 2 cytokines are protective against protozoan infection or promote the pathogenesis induced by protozoans. Thus, we hypothesized that ILC2s are the main source of early type 2 cytokines in the liver during amebic infection.

Here we report that the numbers of ILC2s and type 2 cytokine production were significantly increased during severe ALA formation in Rag2 KO mice. *In vivo* depletion of ILC2s in Rag2 KO mice controlled ALA formation without any difference in IFN-γ production, and *in vivo* ILC2-transfer experiments showed that ILC2s were responsible for severe ALA formation by promoting the accumulation of eosinophils and neutrophils in the liver. Our results demonstrate that ILC2s are the main source of type 2 cytokines in the early phase of ALA and contribute to exacerbating the pathogenesis of ALA.

RESULTS

Increased Numbers of ILC2s and Upregulated Type 2 Cytokines in Rag2 KO Livers after *E. histolytica* Inoculation via the Intraportal Vein

To elucidate whether ILC2s are a source of type 2 cytokines in the early phase of ALA and the role and function of ILC2s in ALA formation, Rag2 knockout (KO) mice, deficient for T cells and B cells, were inoculated with *E. histolytica*, and the kinetics of ILC2s and type 2 cytokine production were monitored. Previous studies injected *E. histolytica* directly into liver parenchyma to mimic ALA (Campbell et al., 1999; Cieslak et al., 1992); however, the injection procedure and injection itself may lead to the release of danger signals such as IL-33. As an alternative method, we induced a natural infection type of ALA by inoculating ameba into the portal vein without damaging the liver parenchyma. To mimic ALA in mice, we infected C57BL/6 (WT) and Rag2 KO mice with 2×10^5 *E. histolytica* via the portal vein without damaging the liver. We used Rag2 KO mice, which are deficient for T and B cells, to specifically investigate the role of ILCs in ALA formation without influence from T and B cells and their production of cytokines. The direct inoculation of *E. histolytica* into a portal vein, which mimics the natural route of metastasis of ameba, led to ALA formation in WT *and* Rag2 KO mice. Figures 1A and S1A show ALA formation as white spots as a gross observation in WT and Rag2 KO livers at day 4 after *E. histolytica* injection. Amebic abscesses were accompanied by the necrosis of hepatocytes and accumulation of leukocytes around amebae in WT and Rag2 KO mice (Figures 1B and S1B). The area and number of abscess in the liver were similar between WT and Rag2 KO mice, suggesting that T and B cells are dispensable for the early phase of ALA formation (Figures 1C and 1D). As Rag2 KO and WT mice developed ALA via the intra-portal injection of ameba, we measured the mRNA expression of type 2 cytokines during ALA formation to examine the involvement of ILC2s. Hepatic IL-5, but not IL-13, mRNA expression was significantly upregulated in WT and Rag2 KO mice on day 4 (Figures 1E and 1F). ILC2s are activated by the epithelial cell-derived cytokines IL-25, IL-33, and TSLP and produce a large amount of IL-5 and IL-13 in the lungs and intestine upon infection with the helminth *Nippostrongylus brasiliensis* (Moro et al., 2010; Neill et al., 2010). We examined the expression of epithelial cell-derived cytokines in the liver. *E. histolytica* injection into WT and Rag2 KO mice enhanced IL-33 mRNA expression on day 4 (Figure 1G); however, IL-25 was not detected (data not shown). Next, we examined the kinetics of ILC2s in the livers of WT and Rag2 KO mice. The hepatic ILC2s were identified as $GATA3^+$, $Thy1.2^+$, $CD45^+$, $lineage^-$, $T1/ST2^+$ cell population. The absolute number of ILC2s in the liver was significantly increased on day 4 in WT and Rag2 KO mice after *E. histolytica* injection (Figures 1H and S2). $IL\text{-}17RB^+$, $KLRG1^+$, $T1/ST2^-$, $CD45^+$, $lineage^-$ cells, which is inflammatory ILC2s, were not detected in this model, suggesting that the hepatic ILC2s that increased during ALA formation were tissue-resident ILC2s. During ALA formation, other innate immune cells in the liver, such as eosinophils and neutrophils were increased and showed similar kinetics in both WT and Rag2 KO mice, whereas NK cells were not significantly increased in either WT or Rag2 KO mice (Figures S3A–S3C). The proportion of neutrophils in blood was significantly increased, whereas the blood eosinophils were significantly decreased in Rag2 KO mice on day 4 compared with uninfected mice (Figures S3D and S3E). The number of ILC2s was increased in the livers of Rag2 KO mice accompanied by the upregulation of type 2 cytokines at the early phase of ALA formation similar to that in WT mice. This indicated that the portal vein injection of *E. histolytica* to Rag2 KO mice is a suitable model of ALA to assess the role of ILC2s in the liver.

[12]Laboratory for Innate Immune Systems, Osaka University Graduate School of Medicine, Osaka, Japan

[13]Lead Contact

*Correspondence: risa-n@nagasaki-u.ac.jp (R.N.), shinjiro@nagasaki-u.ac.jp (S.H.)

https://doi.org/10.1016/j.isci.2020.101544

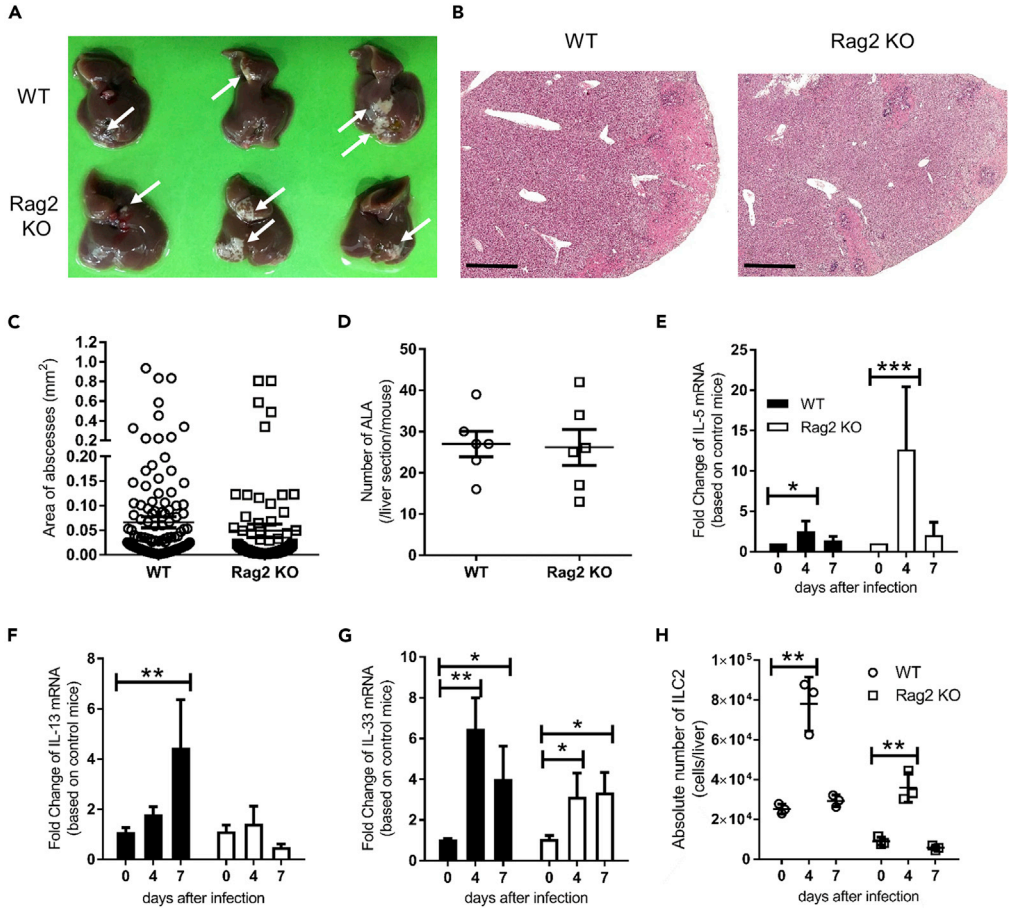

Figure 1. ILC2s Increase in the Livers of WT and Rag2 KO Mice during ALA Formation via Intra-Portal Vein Injection with 2 × 10^5 *E. histolytica*

(A) Macro observation of ALA formation in livers from WT and Rag2 KO mice on day 4. Arrows show a representative abscess in the liver. See also Figure S1A.

(B) Histology of liver tissues from WT and Rag2 KO mice stained with H&E on day 4. Representative figures are shown. Original magnification: × 2.5 and scale bar, 1 mm. See also Figure S1B.

(C and D). The area (C) and number (D) of ALA formed in livers on day 4 (n = 6 per group).

(E–G) Expression of mRNA encoding IL-5 (E), IL-13 (F), and IL-33 (G) in liver tissues on days 4 and 7 (n = 3 per time point in each group).

(H) Absolute number of hepatic ILC2s on days 0 (uninfected), 4, and 7 (n = 3 per time point in each group). Hepatic lymphocytes were stained with markers for ILC2 (lineage$^-$ CD45$^+$ Gata3$^+$ Thy1.2$^+$ T1/ST2$^+$ population) by flow cytometry. Absolute numbers were counted by multiplying the percentage of ILC2s by the absolute number of hepatic lymphocytes. Statistically significant differences between day 0 and indicated time points in each group are indicated with p values (*$p < 0.05$, **$p < 0.01$, ANOVA). Each point shows the mean ± standard deviation (SD). Data are representative of three independent experiments. See also Figures S2, S3, and S7.

Hepatic ILC2s Produce High Levels of IL-5 in WT and Rag2 KO Mice during ALA Formation

To clarify whether ILC2s are a major source of IL-5 and IL-13 in the liver early after *E. histolytica* infection, we isolated hepatic lymphocytes on days 0 (naive), 4, and 7 after *E. histolytica* injection and monitored IL-5 and IL-13-producing ILC2s by intracellular staining. Importantly, hepatic ILC2s spontaneously produced high levels of IL-5 in the setting cultured in the medium alone in WT and Rag2 KO mice on day 4 after *E. histolytica* injection (Figures 2A and S4). The number of hepatic IL-5$^+$ ILC2s were markedly increased on day 4 in WT and Rag2 KO mice (Figure 2B). To examine hepatic ILC2s, we stimulated hepatic lymphocytes with PMA and ionomycin followed by staining with mAbs to ILC2 markers as well as IL-5 and IL-13 on days 4 and 7 after *E. histolytica* injection. In WT and Rag2 KO mice, ILC2s were a major producer of IL-5 in response to PMA and ionomycin (Figures 2C, 2D, and S4). However, IL-13-producing ILC2s were rare in the

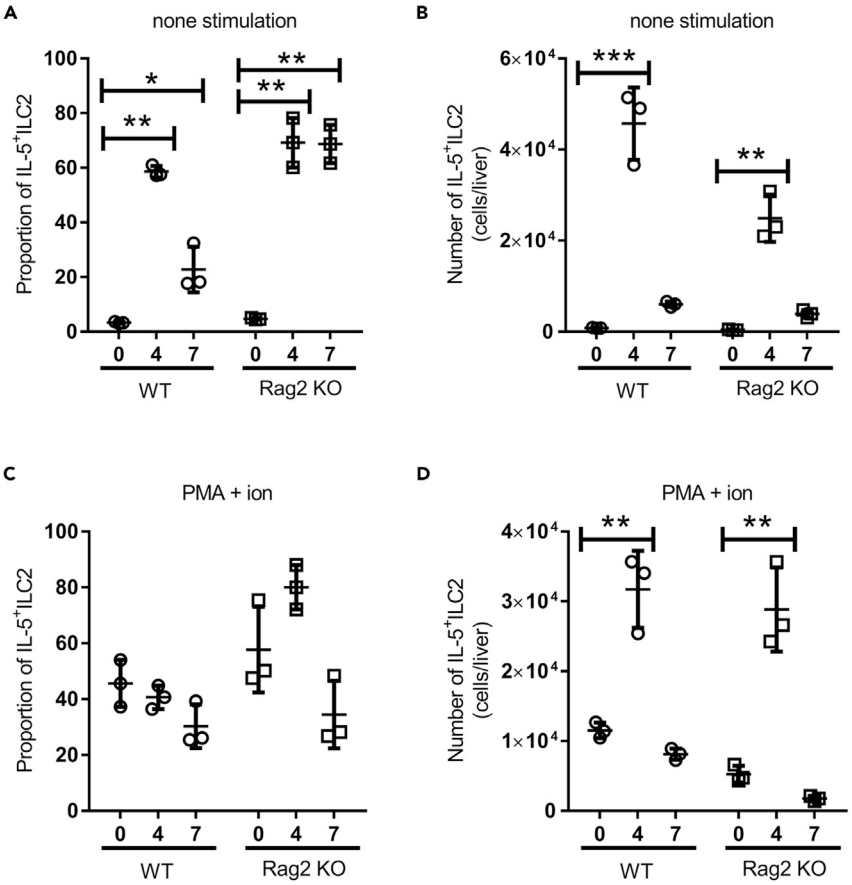

Figure 2. ILC2s Spontaneously Produce High IL-5 Levels in the Livers of WT and Rag2 KO Mice at the Early Phase of ALA Formation

The proportion (A and C) and absolute number (B and D) of IL-5-producing ILC2s in livers from WT and Rag2 KO mice on days 0 (naive), 4, and 7 (n = 3 per time point in each group). Hepatic lymphocytes were stimulated with PMA and ionomycin (C and D; PMA + ion) or were unstimulated (A and B; none stimulation).

Statistically significant differences between day 0 and indicated time points in each group are indicated with p values (*$p < 0.05$, **$p < 0.01$, ***$p < 0.001$, ANOVA). Each point shows the mean ± standard deviation (SD). Data are representative of at least three independent experiments. See also Figure S4.

liver during ALA formation (Figure S4). These results indicated that hepatic ILC2s are a principal source of early IL-5 during ALA formation in WT and Rag2 KO mice.

ALA Development Is Controlled by the *In Vivo* Depletion of ILC2s

It is unclear whether ILC2s exacerbate ALA formation or protect mice from ALA. To clarify the roles of ILC2s in the development of ALA, we depleted ILC2s in the liver by the administration of anti-mouse (α) CD25 mAb into Rag2 KO mice, which lack T and B cells, every 2 days from 3 days before *E. histolytica* injection. Because activated T cells, especially regulatory T (Treg) cells and Th2 cells, also express CD25 on their surface, the *in vivo* administration of αCD25 mAb into Rag2 KO mice is a suitable method to deplete ILCs alone and produce an *in vivo* setting where the presence or absence of ILCs are the major difference between the two groups. We confirmed the substantial reduction of ILC2s in the Rag2 KO liver, whereas there was no difference in the proportion of blood eosinophils, neutrophils, and the absolute number of other immune cells such as NK cells, ILC1s, resident Kupffer cells (KCs), and transient inflammatory monocyte-derived KCs after two doses administration of αCD25 mAb (Figures 3A and S5). IL-17RB$^+$ KLRG1$^+$ T1/ST2$^-$ CD45$^+$ lineage$^-$ inflammatory ILC2 was not detected in the liver treated with αCD25 mAb (data not shown). The number of hepatic ILC2s on day 4 after injection was significantly decreased by αCD25 mAb treatment (Figure 3B). We observed the liver histology on day 4 after *E. histolytica* injection. ILC2-depleted Rag2 KO mice reduced ALA formation compared with control Rag2 KO mice treated with isotype-matched

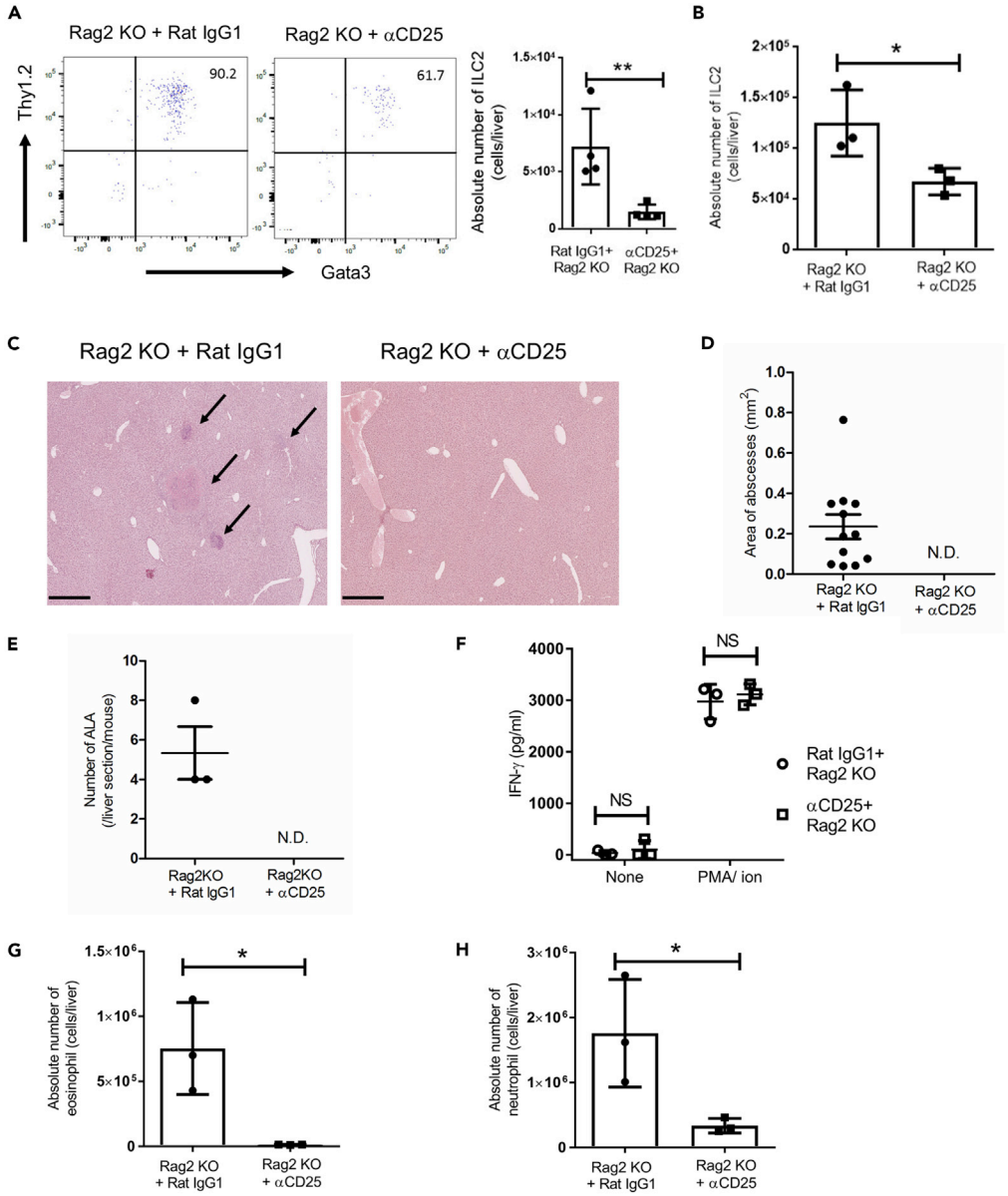

Figure 3. ALA Development Is Better Controlled by the *In Vivo* Depletion of ILC2s in Rag2 KO Mice

(A) Confirmation of *in vivo* ILC2 depletion in the livers of Rag2 KO mice treated with αCD25 mAb or control rat IgG1 by flow cytometry. Hepatic ILC2s were detected after two administrations of αCD25 mAb prior to *E. histolytica* injection. The numbers indicate the percentage of cells in corresponding quadrants.

(B) The absolute number of hepatic ILC2s on day 4 after *E. histolytica* injection.

(C) Histology of liver tissues stained with H&E on day 4. Representative figures are shown. Original magnification: ×5. Scale bar, 500 μm. Arrows show a representative abscess in the liver.

(D and E) The area (D) and number (E) of ALA formed in the liver sections on day 4. The plots in (D) show each area of all ALA observed in three ameba-injected mice. N.D. indicates no detection of abscesses.

(F) ELISA analysis of IFN-γ production by hepatic lymphocytes from ILC2-depleted Rag2 KO mice on day 4. NS indicates no statistical difference.

(G and H) The absolute numbers of eosinophils (G; MHC class II$^-$ SiglecF$^+$ CD11b$^+$ cells), neutrophils (H; CD11b$^+$ Gr-1$^+$ F4/80$^-$ MHC class II$^-$ SiglecF$^-$ cells) on day 4.

Statistically significant differences between control rat IgG1 treated and ILC2-depleted Rag2 KO mice are indicated with p values (*$p < 0.05$, unpaired 2-tailed Student's t test). Each point shows the mean ± standard deviation (SD). Data are representative of at least three independent experiments. See also Figure S5.

mAb (Figure 3C). The area and number of ALA were not detectable in ILC2-depleted Rag2 KO (Figures 3D and 3E). Thus, ALA was controlled by the *in vivo* depletion of ILC2s in Rag2 KO mice, indicating ILC2s are responsible for ALA formation.

ILC2 Depletion Rescues Rag2 KO Mice from Severe ALA without Upregulating IFN-γ Production

IFN-γ has a protective role in innate immunity against ALA in SCID mice (Seydel et al., 2000). As IFN-mediated type 1 and type 2 immune responses are mutually regulated, ILC2s might exacerbate ALA by regulating innate IFN-γ production *in vivo*. To examine the impact of ILC2 depletion on IFN-γ production in the liver, we assessed the ability of hepatic lymphocytes to produce IFN-γ in Rag2 KO with or without ILC2s on day 4 after *E. histolytica* injection. There was no difference in IFN-γ production between ILC2-depleted and control Rag2 KO mice (Figure 3F). This result shows that the control of severe ALA formation observed in ILC2-depleted Rag2 KO mice was not due to the upregulation of IFN-γ production. ILC2-depleted Rag2 KO mice also had significantly fewer eosinophils and neutrophils in the liver compared with control IgG-treated Rag2 KO mice (Figures 3G and 3H). Thus, ILC2s might exacerbate ALA by increasing the numbers of eosinophils and neutrophils in the liver.

ILC2s Directly Exacerbate the Pathogenesis of ALA Accompanied by Eosinophilia and Neutrophilia

To elucidate whether ILC2s contribute directly to the pathogenesis of ALA, we adoptively transferred ILC2s into $Rag2^{-/-}\gamma_c^{-/-}$ mice, which lack ILCs, NK cells, T cells, and B cells. Transferred ILC2s were originally isolated from the mesentery of naive WT mice and possessed the ability to produce IL-5 and IL-13 under IL-33 stimulation (Figures S6A and S6B). Overall, 2×10^6 non-stimulated ILC2s were intravenously transferred into $Rag2^{-/-}\gamma_c^{-/-}$ mice 1 day before the injection of 2×10^5 *E. histolytica*. The transferred ILC2s were confirmed to be in the liver on day 4 after *E. histolytica* injection (Figure S6C). Interestingly, ILC2-transferred $Rag2^{-/-}\gamma_c^{-/-}$ mice developed severe ALA associated with hemorrhagic necrosis in the central part of ALA compared with non-transferred $Rag2^{-/-}\gamma_c^{-/-}$ mice on day 4 after *E. histolytica* injection (Figure 4A). The ILC2 transfer significantly increased the area and number of ALA (Figures 4B and 4C). In this setting, we examined the accumulation of eosinophils and neutrophils and found they were significantly increased in the livers of ILC2-transferred $Rag2^{-/-}\gamma_c^{-/-}$ mice on day 4 (Figures 4D and 4E). These results suggest that ILC2s exacerbate the pathogenesis of ALA accompanied by eosinophilia and neutrophilia.

IL-33 Is a Trigger of ILC2-Mediated ALA Formation

Next, we investigated how ILC2s are activated to exacerbate the pathogenesis of ALA after ameba injection. As IL-33, but not IL-25, mRNA expression was profoundly upregulated in the liver (Figure 1G), we clarified whether IL-33 is crucial for the activation of ILC2s, which exacerbate ALA. $IL\text{-}33^{GFP/GFP}$ mice, which lack IL-33 protein expression, showed reduced ALA formation compared with WT mice on day 4 after *E. histolytica* injection (Figures 5A and 5C). In IL-33-deficient mice, large ALA (>0.2 mm^2) were not observed, whereas they were scattered throughout the liver in WT mice (Figure 5B). To examine the localization of ILC2s in the liver in detail, prior to the pathogen exposure and during acute *E. histolytica* infection, immunofluorescent staining of frozen tissue sections was performed. As shown in Figure 6A, in both naive WT and Rag2 KO mice, some ILC2s identified by strong red signal (T1/ST2) and blue signal (Gata3) were only detected in portal triad area in liver lobule. It is known that WT liver contains tissue-resident Tregs, which expressed Gata3 and T1/ST2 (Popovic et al., 2017). However, the similar strong Gata3 high, T1/ST2 high signal and localization of ILC2s were observed in both WT and Rag2 KO mice, indicating the Gata3 and T1/ST2 double-positive cells were not tissue-resident liver Tregs. In infected liver on day 7 post infection, ILC2s were observed within the necrotic lesions of ALA and surrounding inflammatory areas filled with $IL\text{-}33^+$ cells in green signal (Figures 6B–6D). In both uninfected and infected phases, the close physical juxtaposition of ILC2 and $IL\text{-}33^+$ cell is well revealed. It should be noted that the strong red signal from ILC2 merges to green of $IL\text{-}33^+$ cell to generate yellow signal shown in detail region of Figures 6C and 6D. It is still unclear so far what type of cells produce IL-33 in this model. But, given that IL-33 is a key activator of ILC2s, it is possible that ILC2s recruited to the lesion are the critical trigger cell in the pathogenesis of ALA.

IL-5 Leads to the Development of ALA Accompanied by Eosinophil Accumulation

To clarify whether IL-5 directly contributes to the pathogenesis of ALA, we analyzed ALA formation in Rag2 KO mice after neutralizing IL-5 with anti-IL-5 mAb. ALA formation was reduced in anti-IL-5-treated mice

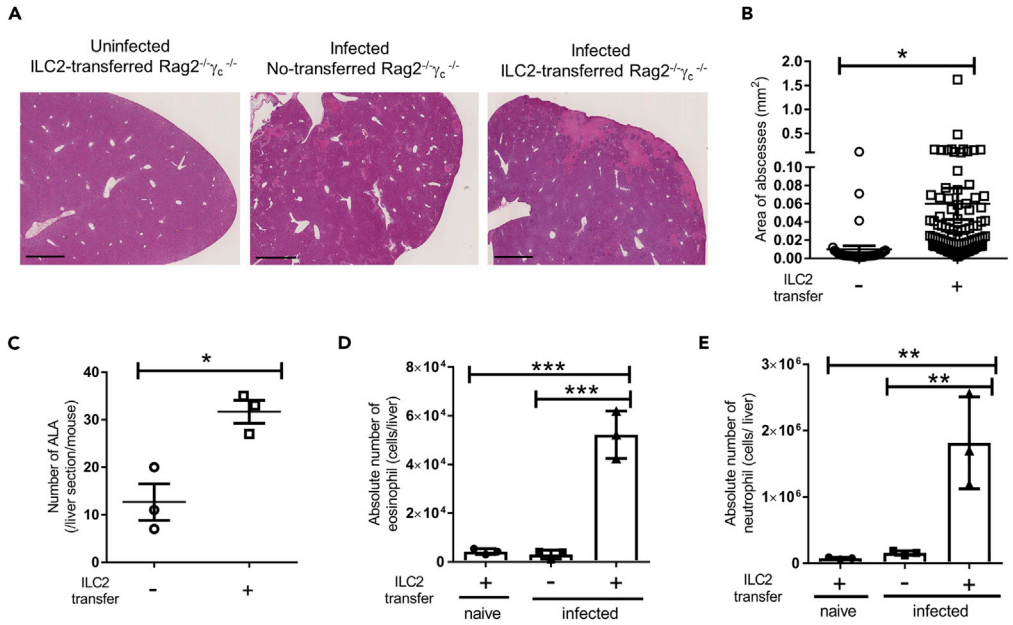

Figure 4. ILC2-Transferred Rag2$^{-/-}\gamma_c^{-/-}$ KO Mice Develop Severe ALA Accompanied by the Accumulation of Eosinophils and Neutrophils in the Liver

Naive ILC2s (2 × 10^6) were transferred into Rag2$^{-/-}\gamma c^{-/-}$ (DKO) mice 1 day before *E. histolytica* injection

(A) Histology of liver tissues stained with H&E on day 4 after *E. histolytica* injection. Representative figures are shown. Original magnification: ×2.5. Scale bar, 1 mm. Each group consisted of three mice.

(B and C) The area (B) and number (C) of ALA formed in liver sections from DKO mice with or without ILC2 transfer on day 4 (*$p < 0.05$, unpaired 2-tailed Student's t test, n = 3 per group).

(D and E) The absolute numbers of eosinophils (D) and neutrophils (E) in livers from DKO with or without ILC2 transfer on day 4 (n = 3 per group).

Statistically significant differences between ILC2-transferred and non-transferred DKO mice are indicated with p value (**$p < 0.01$, ***$p < 0.001$, ANOVA). Each point shows the mean ± standard deviation (SD). Data are representative of at least two independent experiments. See also Figure S6.

(Figure 7A). The area and number of ALA were markedly decreased in anti-IL-5-treated Rag2 KO mice compared with WT mice (Figures 7A–7C). Eosinophil accumulation in the liver was significantly decreased in anti-IL-5-treated Rag2 KO mice compared with rat IgG1 treated Rag2 KO mice (Figure 7D). However, in this setting, there was no difference in the absolute number of ILC2s and neutrophils in the livers between groups (Figures 7E and 7F). These results suggest that IL-5 produced by ILC2s induces eosinophil accumulation, which then exacerbates ALA.

DISCUSSION

In this study, ILC2s were identified as the main source of type 2 cytokines in early ALA formation. Furthermore, type 2 cytokine-producing ILC2s exacerbated the pathology of ALA formation in mice injected with ameba via the portal vein.

To specifically investigate the role of innate immune cells in ALA formation, we used WT and Rag2 KO mice, which are deficient for T and B cells. In WT and Rag2 KO mice, similar levels of ALA formation were observed in the early phase and the number of hepatic ILC2s producing high levels of IL-5 was significantly increased on day 4 after *E. histolytica* injection. This implies that innate immune cells, in particular, ILC2s, but not T and B cells, are strongly involved in the pathogenesis of ALA.

ILC2s are tissue-resident cells that expand locally and produce abundant IL-5 and IL-13 in non-lymphoid organs such as the lungs and small intestine, and the mesenteric lymph nodes during the acute phase of *Nippostrongylus brasiliensis* infection (Gasteiger et al., 2015; Moro et al., 2016). On day 7 after *E. histolytica* injection, the number of ILC2s and IL-5-producing ILC2s were diminished in the liver. As ALA formation peaks on day 4 and injected mice can survive with recovery from ALA in this experimental

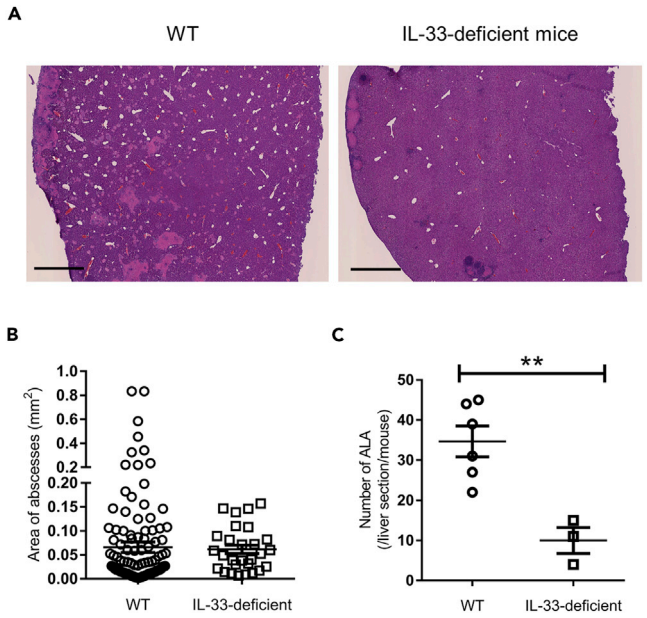

Figure 5. IL-33-Deficient Mice Show Less ALA Formation Compared with WT Mice

IL-33$^{GFP/GFP}$ (IL-33-deficient) mice were injected with 2 × 10^5 *E. histolytica*.

(A) Histology of liver tissues stained with H&E on day 4. Representative figures are shown. Original magnification: ×2.5. Scale bar, 1 mm.

(B and C) The area (B) and number (C) of ALA formed in liver sections from WT (n = 6) and IL-33-deficient mice (n = 3) on day 4. **p < 0.01, unpaired 2-tailed Student's t test.

model, the decrease of the number and function of ILC2s on day 7 may correlate with the recovery from ALA. After *E. histolytica* injection, IL-13 mRNA expression was augmented in the livers of WT, but not Rag2 KO, mice on day 7. We did not detect a significant increase in IL-13-producing ILC2s in the livers of WT and Rag2 KO mice on day 4 even after *ex vivo* stimulation with PMA and ionomycin. It is possible from these results that IL-13 production is dependent on conventional T cells after ameba infection.

IFN-γ is critical for clearing ameba from the liver and suppressing the function and proliferation of ILC2s (Mchedlidze et al., 2016; Moro et al., 2016). In ILC2-depleted Rag2 KO mice, levels of IFN-γ production were similar to that in WT mice. Thus, IFN-γ production in the liver was not affected by ILC2 depletion, suggesting that ILC2s exacerbate the pathology of ALA without changing the production of IFN-γ in the microenvironment.

How IL-5 is involved in the pathogenesis of ALA is currently unclear. In this study, we neutralized IL-5 *in vivo* to clearly show that IL-5 exacerbated ALA progression. IL-5 produced by ILC2s induced the survival and proliferation of eosinophils, which lead to eosinophilia (Nussbaum et al., 2013). In a susceptible mouse model of ALA, severe abscesses were mainly mediated by eosinophils that strongly infiltrated into the abscess (Estrada-Villasenor et al., 2007), indicating that ILC2-produced IL-5 directly induces eosinophil infiltration that helps to form severe ALA around *E. histolytica*.

In this study, we focused on the accumulation of eosinophils and neutrophils during ILC2-mediated ALA formation. The kinetics of eosinophils and neutrophils in the blood were inconsistent with those of liver eosinophils and neutrophils, suggesting that the size and composition of the ALA do not simply reflect the levels of neutrophils and eosinophils in the blood. Although systemic changes are induced after ameba injection, the pathology observed during ALA is not the simple reflection of such systemic changes. Other immune cells activated by ILC2s may also be involved in the pathogenesis of ALA. It was reported that IL-5 increased the number of alternatively activated macrophages and fibroblasts (Reiman et al., 2006). In a hamster model of ALA caused by *E. nuttalli*, which is highly prevalent in macaques, alternatively activated macrophages were increased in the liver in the late stage of abscess progression (Guan et al., 2018). Thus, alternatively activated macrophages augmented by IL-5 might contribute to the pathology of ALA

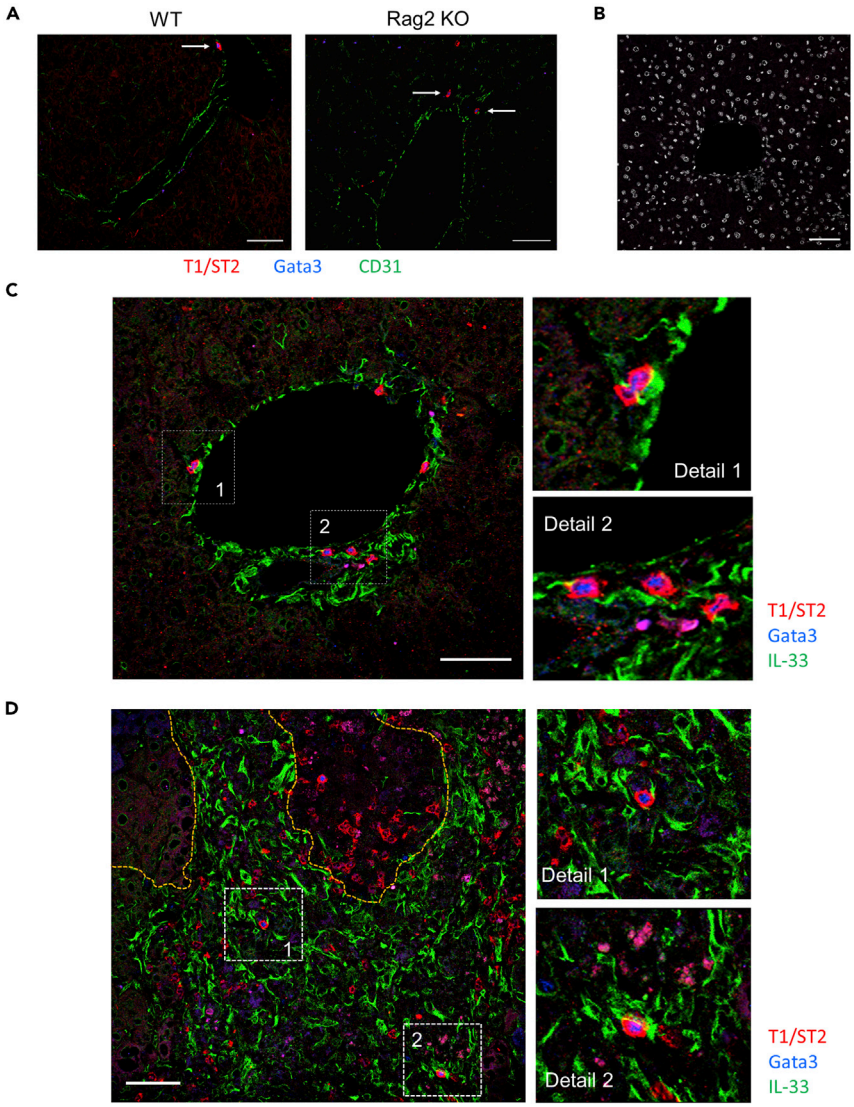

Figure 6. Localization of ILC2s and IL-33^{+} Cells in the Liver after Ameba Injection

(A) The liver sections from uninfected WT and Rag2 KO mice were stained with anti-T1/ST2 (red), anti-Gata3 (blue), and anti-CD31 (green) mAbs.

(B) Immunofluorescent staining with isotype control Ab and DAPI (white).

(C) The liver section from uninfected WT mice was stained for ILC2s and IL-33^{+} cells with anti-T1/ST2 (red), anti-Gata3 (blue), and anti-IL-33 (green) mAbs.

(D) The liver section from infected WT mice was stained for ILC2s and IL-33^{+} cells using anti-T1/ST2 (red), Gata3 (blue), and IL-33 (green) mAbs. Scale bar, 50 μm. Yellow dotted lines show the necrotic lesion of ALA. Numbers in white dotted squares show further detail on the right images as detail 1 and 2. Results are representative of three sections from three mice examined.

caused by *E. histolytica*. We need to clarify further the involvement of alternatively activated macrophages in ILC2-mediated ALA.

The adoptive transfer of naive ILC2s into Rag2$^{-/-}\gamma_c^{-/-}$ KO mice clearly showed that ILC2s exacerbated the pathogenesis of ALA accompanied by the augmented accumulation of neutrophils. Recently it was reported that ILC2 subpopulation exhibited the conversion into IL-17-producing cells in response to IL-1β and IL-23 (Bernink et al., 2019; Hochdorfer et al., 2019). As IL-17 induces the migration of neutrophils into the site of infection, ILC2 plasticity into IL-17-producing cells may provide a possibility to increase the accumulation of neutrophils in the liver. A previous study reported that IL-33 inoculated into the ears

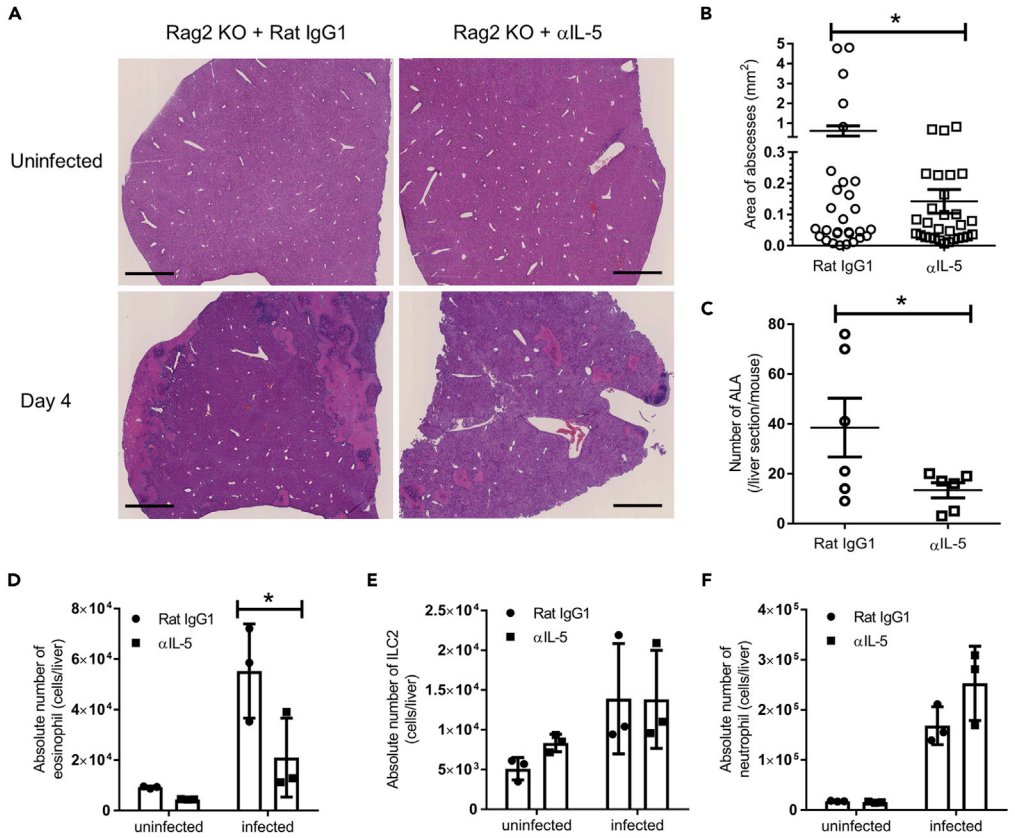

Figure 7. ALA Formation Is Regulated by IL-5 with the Accumulation of Eosinophils in Rag2 KO Mice

Rag2 KO mice were intraperitoneally administered 250 μg/mouse anti-(α) IL-5 mAb every 2 days from 3 days before *E. histolytica* injection (day −3, −1, 1, and 3).

(A) Histology of liver tissues stained with H&E on day 4 after *E. histolytica* injection. Representative figures are shown. Original magnification: ×2.5. Scale bar, 1 mm.

(B and C) The area (B) and number (C) of ALA formed in liver sections from Rag2 KO mice treated with αIL-5 mAb or control rat IgG1 on day 4 (*$p < 0.05$, unpaired 2-tailed Student's t test, n = 6 per group). The plots in (B) show each area of all ALA observed in six mice per group.

(D–F) The absolute numbers of eosinophils (D), hepatic ILC2s (E) and neutrophils (F) on day 4 (n = 3 per group). Statistically significant differences between isotype control Ab treated-Rag2 KO and IL-5 depleted-Rag2 KO mice are indicated with p value (*$p < 0.05$, unpaired two-tailed Student's t test). Each point shows the mean ± standard deviation (SD). Data are representative of at least three independent experiments.

of mice induced inflammatory psoriatic lesions accompanied by the recruitment of neutrophils into the ear after phorbol ester challenge. Recruited neutrophils produced large amounts of the chemokine KC (CXCL1) in the inflammatory ear lesions (Lefrancais et al., 2012). Because IL-33-deficient mice showed less ALA formation, IL-33 is likely responsible for the initiation of ALA formation. We noted that there was a trend of the co-localization of ILC2 and IL-33$^+$ cell in the liver from naive and infected mice. As hepatic ILC2s infiltrated around ALA accompanied by the interaction with a lot of IL-33$^+$ cells, suggesting a possibility that IL-33 activates ILC2s and induces the accumulation of neutrophils, which then produce chemokines and/or other inflammatory factors involved in liver inflammation and subsequently severe ALA. However, to date, it is unclear whether neutrophils are responsible for ALA formation in this setting and whether ILC2s activated by IL-33 are associated with the function of neutrophils. Further investigations are required to reveal the relevance of ILC2s and neutrophils to ALA.

A number of studies about the immune response against protozoan parasitic diseases such as leishmaniasis, malaria, and toxoplasmosis have revealed the role of type 1 immunity in controlling the infection. Regarding type 2 immunity in protozoan infection, a few studies reported that type 2 immunity provided the susceptibility to leishmanial infection and protected against cerebral malaria via IL-33-mediated

ILC2, M2 macrophages, and Tregs (Besnard et al., 2015). Our study has revealed the involvement of ILC2s during a protozoan infection and the contributions of ILC2s in the pathogenesis of liver abscesses caused by *E. histolytica*. To date, few studies have investigated the function of ILC2s in the liver. One study reported that ILC2s exacerbated Con A-induced hepatitis in mice, and another clarified the association between increased ILC2s and human liver fibrosis (Gonzalez-Polo et al., 2019; Zhang et al., 2019). Consistent with previous studies, we clearly demonstrated that ILC2s exacerbate ALA caused by *E. histolytica*.

In conclusion, we showed that ILC2s are a major source of early type 2 cytokines, such as IL-5, during ALA formation and that they contribute to the exacerbation of ALA accompanied by the accumulation of eosinophils and neutrophils. Furthermore, IL-33-deficient and IL-5-neutralized mice revealed the mechanism of ILC2-mediated ALA formation in which IL-5-producing ILC2s activated by IL-33 exacerbated ALA. Further studies are required to clarify how ILC2s induce severe ALA via eosinophils and neutrophils and/or other immune cells and whether IL-5-producing ILC2s have functional relevance to neutrophil accumulation in the pathogenesis of ALA.

Limitations of the Study

In this study, we indicated that ILC2s contribute to the pathogenesis of ALA at the early phase of the disease using a mouse model inoculated with *E. histolytica* via the hepatic portal vein. The present animal model of ALA may provide a concern about the physiological relevance about the portal vein inoculation. However, there is no way for the natural infection model via oral to develop ALA so far, much less a translocation model of *E. histolytica* trophozoites to the liver from the intestine. To mimic the translocation of ameba for the natural occurring of ALA, we used the portal vein inoculation model in which we can avoid the damage of liver parenchyma that may lead to the production of IL-33 and other alarmins. ILC2s can produce abundant type 2 cytokines, but the number and proportion of ILC2s are much lower compared with T cell at steady state. To monitor the kinetics and role of ILC2s, we used Rag2 KO mice (T cell-deficient mice) to exclude type 2 responses by Th2 cell. We confirmed that both WT (under the presence of T cells) and Rag2 KO mice developed a similar level of ALA formation on day 4. This result clearly indicated that T cell does not influence the development and pathogenesis of ALA at least at this time point. Although we suggest ILC2s exacerbate amebic liver abscess in mice, we should consider the balance between ILC2s and T cell in immunocompetent mice. In flow cytometry analysis, we could not exclude dead cells by the specific staining owing to the limitation of detectors in the flow cytometer. As hepatic ILC2s do not have a specific marker, the identification of hepatic ILC2s needs staining of a number of surface and intracellular markers. Since our study made it a priority to stain these markers for detecting hepatic ILC2s, a detector of flow cytometer did not remain for dead cell staining. Instead of the specific staining for live/ dead cell discrimination, dead cells were distinguished by gating on the FSC/SSC plot. ILC2 depletion in Rag2 KO mice rescued ALA formation without any difference in IFN-γ production on day 4. It remains the possibility that IFN-γ production by ILC1s may occur much earlier time point than on day 4. We could not examine it owing to the restriction of outing by COVID-19 pandemic. So far, the roles and functions of ILC1s in ALA formation remain unclear. We need further investigations to reveal the relevance of ILC1s and ILC2s at the early time point of ALA.

Resource Availability

Lead Contact

Further information and requests for resources and reagents should be directed to and will be fulfilled by the Lead Contact, Shinjiro Hamano (shinjiro@nagasaki-u.ac.jp).

Materials Availability

This study did not generate new unique reagents.

Data and Code Availability

The published article includes all data generated or analyzed during this study. Any additional information will be available from the lead contact upon request.

METHODS

All methods can be found in the accompanying Transparent Methods supplemental file.

SUPPLEMENTAL INFORMATION

Supplemental Information can be found online at https://doi.org/10.1016/j.isci.2020.101544.

ACKNOWLEDGMENTS

The authors are grateful to Megumi Hamasaki and Hiromi Oda for breeding, genotyping, maintenance, and care of the mice used in this study. We also thank Fumie Hara for technical assistance. This study was conducted at the Joint Usage/Research Center on Tropical Disease, Institute of Tropical Medicine, Nagasaki University, Japan. This study was supported by a Grant-in-Aid for Young Scientists (B) JP16K19118 to R.N. from the Japan Society for the Promotion of Science (JSPS), a Grant-in-Aid for Scientific Research on Priority Areas from MEXT (21022037 to S.H.), Grants-in-Aid for International Scientific Research (B) from JSPS (23406009 and 26305013 to S.H.). The funders had no role in study design, data collection and analysis, decision to publish, or preparation of the manuscript. We thank Edanz Group (www.edanzediting.com/ac) for editing a draft of this manuscript.

AUTHOR CONTRIBUTIONS

R.N. designed this study, analyzed the data, and wrote the manuscript. R.N. and S.D. maintained amebae and performed the experiments. A.Y. supported and performed the immunofluorescence of the liver. T.M. supported culture of amebae and performed antibody administration for revised experiments. S.K. and K.M. provided protocols for ILC2 analysis and *in vitro* culture of ILC2s and data interpretation. M.K. supported the analysis of real-time PCR data and advised the manuscript. M.S. made histological sections of the liver. S.H., K.M., and S.K. participated in the preparation and the edition of the manuscript.

DECLARATION OF INTERESTS

The authors declare no competing interests.

Received: December 30, 2019
Revised: July 24, 2020
Accepted: September 4, 2020
Published: September 25, 2020

REFERENCES

Bernink, J.H., Ohne, Y., Teunissen, M.B.M., Wang, J., Wu, J., Krabbendam, L., Guntermann, C., Volckmann, R., Koster, J., Van Tol, S., et al. (2019). c-Kit-positive ILC2s exhibit an ILC3-like signature that may contribute to IL-17-mediated pathologies. Nat. Immunol. *20*, 992–1003.

Besnard, A.G., Guabiraba, R., Niedbala, W., Palomo, J., Reverchon, F., Shaw, T.N., Couper, K.N., Ryffel, B., and Liew, F.Y. (2015). IL-33-mediated protection against experimental cerebral malaria is linked to induction of type 2 innate lymphoid cells, M2 macrophages and regulatory T cells. PLoS Pathog. *11*, e1004607.

Campbell, D., Gaucher, D., and Chadee, K. (1999). Serum from *Entamoeba histolytica*-infected gerbils selectively suppresses T cell proliferation by inhibiting interleukin-2 production. J. Infect. Dis. *179*, 1495–1501.

Cervantes-Rebolledo, C., Moreno-Mendoza, N., Morales-Montor, J., De La Torre, P., Laclette, J.P., and Carrero, J.C. (2009). Gonadectomy inhibits development of experimental amoebic liver abscess in hamsters through downregulation of the inflammatory immune response. Parasite Immunol. *31*, 447–456.

Cieslak, P.R., Virgin, H.W.T., and Stanley, S.L., Jr. (1992). A severe combined immunodeficient (SCID) mouse model for infection with *Entamoeba histolytica*. J. Exp. Med. *176*, 1605–1609.

Denis, M., and Chadee, K. (1989a). Cytokine activation of murine macrophages for in vitro killing of *Entamoeba histolytica* trophozoites. Infect. Immun. *57*, 1750–1756.

Denis, M., and Chadee, K. (1989b). Human neutrophils activated by interferon-gamma and tumour necrosis factor-alpha kill *Entamoeba histolytica* trophozoites in vitro. J. Leukoc. Biol. *46*, 270–274.

Estrada-Villasenor, E., Morales-Montor, J., Rodriguez-Dorantes, M., Ramos-Martinez, E., Nequiz-Avendano, M., and Ostoa-Saloma, P. (2007). IL-6 KO mice develop experimental amoebic liver infection with eosinophilia. J. Parasitol. *93*, 1424–1428.

Gasteiger, G., Fan, X., Dikiy, S., Lee, S.Y., and Rudensky, A.Y. (2015). Tissue residency of innate lymphoid cells in lymphoid and nonlymphoid organs. Science *350*, 981–985.

Ghadirian, E., and Salimi, A. (1993). In vitro effect of recombinant interferon gamma in combination with LPS on amoebicidal activity of murine Kupffer cells. Immunobiology *188*, 203–219.

Gonzalez-Polo, V., Pucci-Molineris, M., Cervera, V., Gambaro, S., Yantorno, S.E., Descalzi, V., Tiribelli, C., Gondolesi, G.E., and Meier, D. (2019). Group 2 innate lymphoid cells exhibit progressively higher levels of activation during worsening of liver fibrosis. Ann. Hepatol. *18*, 366–372.

Guan, Y., Feng, M., Min, X., Zhou, H., Fu, Y., Tachibana, H., and Cheng, X. (2018). Characteristics of inflammatory reactions during development of liver abscess in hamsters inoculated with *Entamoeba nuttalli*. PLoS Negl. Trop. Dis. *12*, e0006216.

Halim, T.Y., Krauss, R.H., Sun, A.C., and Takei, F. (2012). Lung natural helper cells are a critical source of Th2 cell-type cytokines in protease allergen-induced airway inflammation. Immunity *36*, 451–463.

Hamano, S., Cherry, J., Demmlar-Harrison, J.G., Kaplan, S., Steinbach, J.W., and Hotez, J.P. (2013). Amebiasis. Feigin and Cherrys's Textbook of Pediatric Infectious Diseases (Elsevier).

Haque, R., Huston, C.D., Hughes, M., Houpt, E., and Petri, W.A., Jr. (2003). Amebiasis. N. Engl. J. Med. *348*, 1565–1573.

Hochdorfer, T., Winkler, C., Pardali, K., and Mjosberg, J. (2019). Expression of c-Kit discriminates between two functionally distinct subsets of human type 2 innate lymphoid cells. Eur. J. Immunol. *49*, 884–893.

Houpt, E.R., Glembocki, D.J., Obrig, T.G., Moskaluk, C.A., Lockhart, L.A., Wright, R.L., Seaner, R.M., Keepers, T.R., Wilkins, T.D., and Petri, W.A., Jr. (2002). The mouse model of amebic colitis reveals mouse strain susceptibility to infection and exacerbation of disease by CD4+ T cells. J. Immunol. *169*, 4496–4503.

Kotloff, K.L., Nataro, J.P., Blackwelder, W.C., Nasrin, D., Farag, T.H., Panchalingam, S., Wu, Y., Sow, S.O., Sur, D., Breiman, R.F., et al. (2013). Burden and aetiology of diarrhoeal disease in infants and young children in developing countries (the Global Enteric Multicenter Study, GEMS): a prospective, case-control study. Lancet *382*, 209–222.

Lefrancais, E., Roga, S., Gautier, V., Gonzalez-De-Peredo, A., Monsarrat, B., Girard, J.P., and Cayrol, C. (2012). IL-33 is processed into mature bioactive forms by neutrophil elastase and cathepsin G. Proc. Natl. Acad. Sci. U S A *109*, 1673–1678.

Lotter, H., Jacobs, T., Gaworski, I., and Tannich, E. (2006). Sexual dimorphism in the control of amebic liver abscess in a mouse model of disease. Infect. Immun. *74*, 118–124.

Mchedlidze, T., Kindermann, M., Neves, A.T., Voehringer, D., Neurath, M.F., and Wirtz, S. (2016). IL-27 suppresses type 2 immune responses in vivo via direct effects on group 2 innate lymphoid cells. Mucosal Immunol. *9*, 1384–1394.

Moro, K., Kabata, H., Tanabe, M., Koga, S., Takeno, N., Mochizuki, M., Fukunaga, K., Asano, K., Betsuyaku, T., and Koyasu, S. (2016). Interferon and IL-27 antagonize the function of group 2 innate lymphoid cells and type 2 innate immune responses. Nat. Immunol. *17*, 76–86.

Moro, K., Yamada, T., Tanabe, M., Takeuchi, T., Ikawa, T., Kawamoto, H., Furusawa, J., Ohtani, M., Fujii, H., and Koyasu, S. (2010). Innate production of T(H)2 cytokines by adipose tissue-associated c-Kit(+)Sca-1(+) lymphoid cells. Nature *463*, 540–544.

Motomura, Y., Morita, H., Moro, K., Nakae, S., Artis, D., Endo, T.A., Kuroki, Y., Ohara, O., Koyasu, S., and Kubo, M. (2014). Basophil-derived interleukin-4 controls the function of natural helper cells, a member of ILC2s, in lung inflammation. Immunity *40*, 758–771.

Murray, C.J., Vos, T., Lozano, R., Naghavi, M., Flaxman, A.D., Michaud, C., Ezzati, M., Shibuya, K., Salomon, J.A., Abdalla, S., et al. (2012). Disability-adjusted life years (DALYs) for 291 diseases and injuries in 21 regions, 1990-2010: a systematic analysis for the Global Burden of Disease Study 2010. Lancet *380*, 2197–2223.

Neill, D.R., Wong, S.H., Bellosi, A., Flynn, R.J., Daly, M., Langford, T.K., Bucks, C., Kane, C.M., Fallon, P.G., Pannell, R., et al. (2010). Nuocytes represent a new innate effector leukocyte that mediates type-2 immunity. Nature *464*, 1367–1370.

Nussbaum, J.C., Van Dyken, S.J., Von Moltke, J., Cheng, L.E., Mohapatra, A., Molofsky, A.B., Thornton, E.E., Krummel, M.F., Chawla, A., Liang, H.E., and Locksley, R.M. (2013). Type 2 innate lymphoid cells control eosinophil homeostasis. Nature *502*, 245–248.

Popovic, B., Golemac, M., Podlech, J., Zeleznjak, J., Bilic-Zulle, L., Lukic, M.L., Cicin-Sain, L., Reddehase, M.J., Sparwasser, T., Krmpotic, A., and Jonjic, S. (2017). IL-33/ST2 pathway drives regulatory T cell dependent suppression of liver damage upon cytomegalovirus infection. PLoS Pathog. *13*, e1006345.

Prakash, V., and Bhimji, S.S. (2017). Abscess, Amebic Liver (StatPearls Publishing).

Ravdin, J.I. (1988). Human infection by *Entamoeba histolytica*. In Amebiasis, J.I. RAVDIN, ed. (New York. Edinburgh: Churchill Livingstone), pp. 594–613.

Reiman, R.M., Thompson, R.W., Feng, C.G., Hari, D., Knight, R., Cheever, A.W., Rosenberg, H.F., and Wynn, T.A. (2006). Interleukin-5 (IL-5) augments the progression of liver fibrosis by regulating IL-13 activity. Infect. Immun. *74*, 1471–1479.

Salata, R.A., Murray, H.W., Rubin, B.Y., and Ravdin, J.I. (1987). The role of gamma interferon in the generation of human macrophages cytotoxic for *Entamoeba histolytica* trophozoites. Am. J. Trop. Med. Hyg. *37*, 72–78.

Seydel, K.B., Smith, S.J., and Stanley, S.L., Jr. (2000). Innate immunity to amebic liver abscess is dependent on gamma interferon and nitric oxide in a murine model of disease. Infect. Immun. *68*, 400–402.

Zhang, Y., Qi, C., Li, L., Hua, S., Zheng, F., Gong, F., and Fang, M. (2019). CD8(+) T cell/IL-33/ILC2 axis exacerbates the liver injury in Con A-induced hepatitis in T cell-transferred Rag2-deficient mice. Inflamm. Res. *68*, 75–91.

iScience, Volume *23*

Supplemental Information

Group 2 Innate Lymphoid Cells Exacerbate Amebic Liver Abscess in Mice

Risa Nakamura, Akihiro Yoshizawa, Taeko Moriyasu, Sharmina Deloer, Masachika Senba, Mihoko Kikuchi, Shigeo Koyasu, Kazuyo Moro, and Shinjiro Hamano

Supplemental figure 1

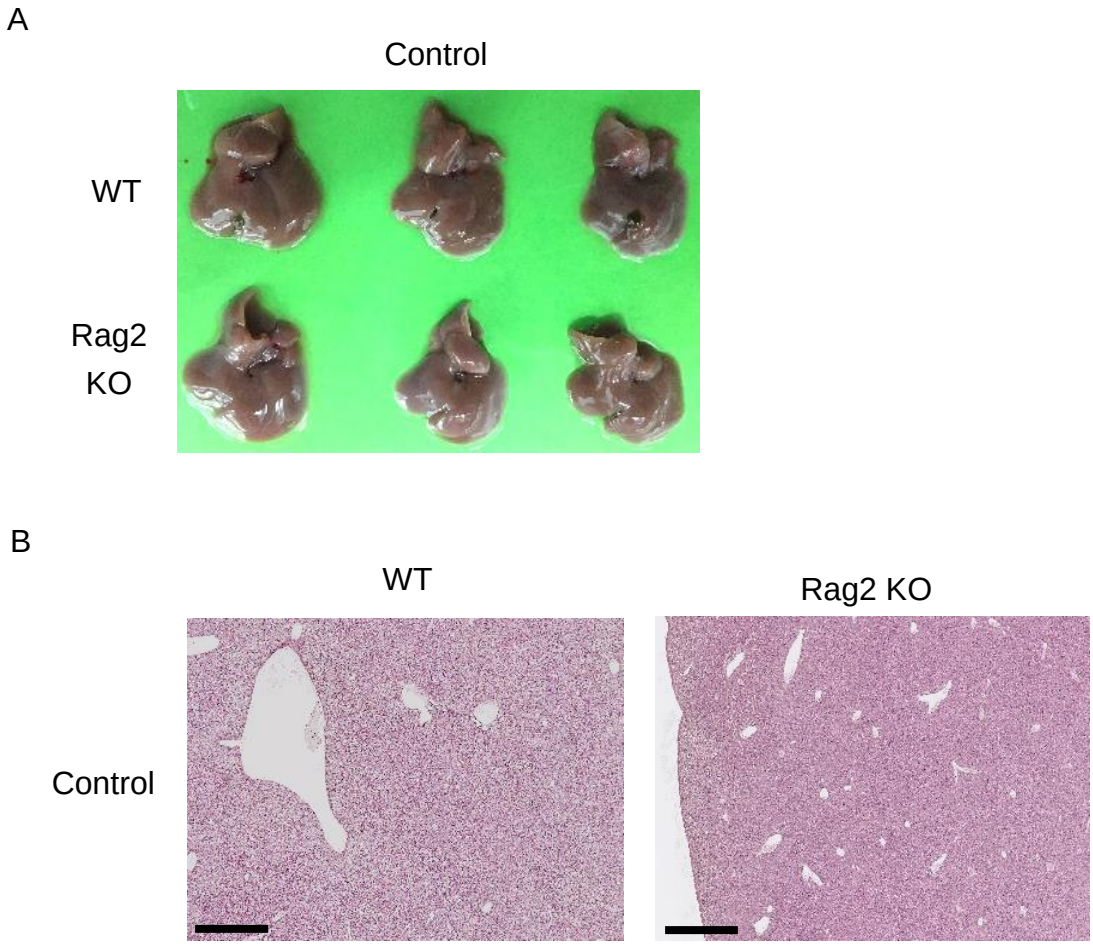

Supplemental figure 1. The observation of the livers from control WT and Rag2 KO mice. Related to Figure 1. (A) Macro observation of the livers from uninfected WT and Rag2 KO mice as a negative control (n = 3). (B) Histology of liver tissues from uninfected WT and Rag2 KO mice stained with H&E. Representative figures are shown. Original magnification: × 2.5 and Scale bar = 1 mm.

Supplemental figure 2

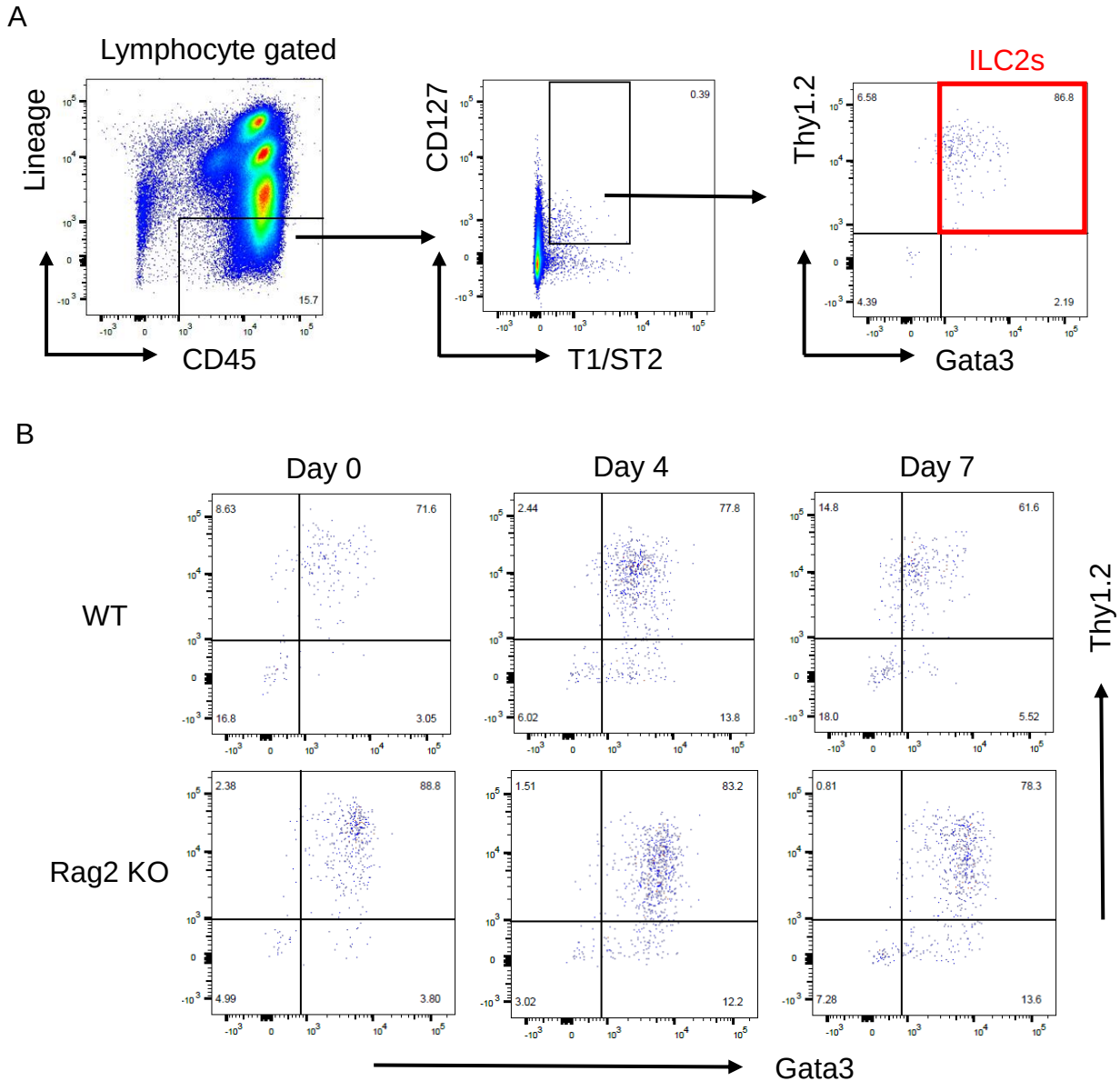

Supplemental figure 2. The kinetics of ILC2s in the livers from WT and Rag2 KO mice after *E. histolytica* injection. Related to Figure 1. Hepatic lymphocytes were collected from WT and Rag2 KO mice on day 0 (naïve), 4 and 7 after *E. histolytica* injection. (A) Gating strategy of hepatic ILC2s in naïve WT mice by flow cytometry. Hepatic ILC2s were detected as a lineage$^-$ CD45$^+$ Gata3$^+$ Thy1.2$^+$ T1/ST2$^+$ gated population. A red square on the dot plot showed hepatic ILC2s. (B) Flow cytometry of hepatic ILC2s in WT and Rag2 KO mice after *E. histolytica* injection. Representative dot plots are shown after gating as in (A). Data are representative of three independent experiments with similar results.

Supplemental figure 3

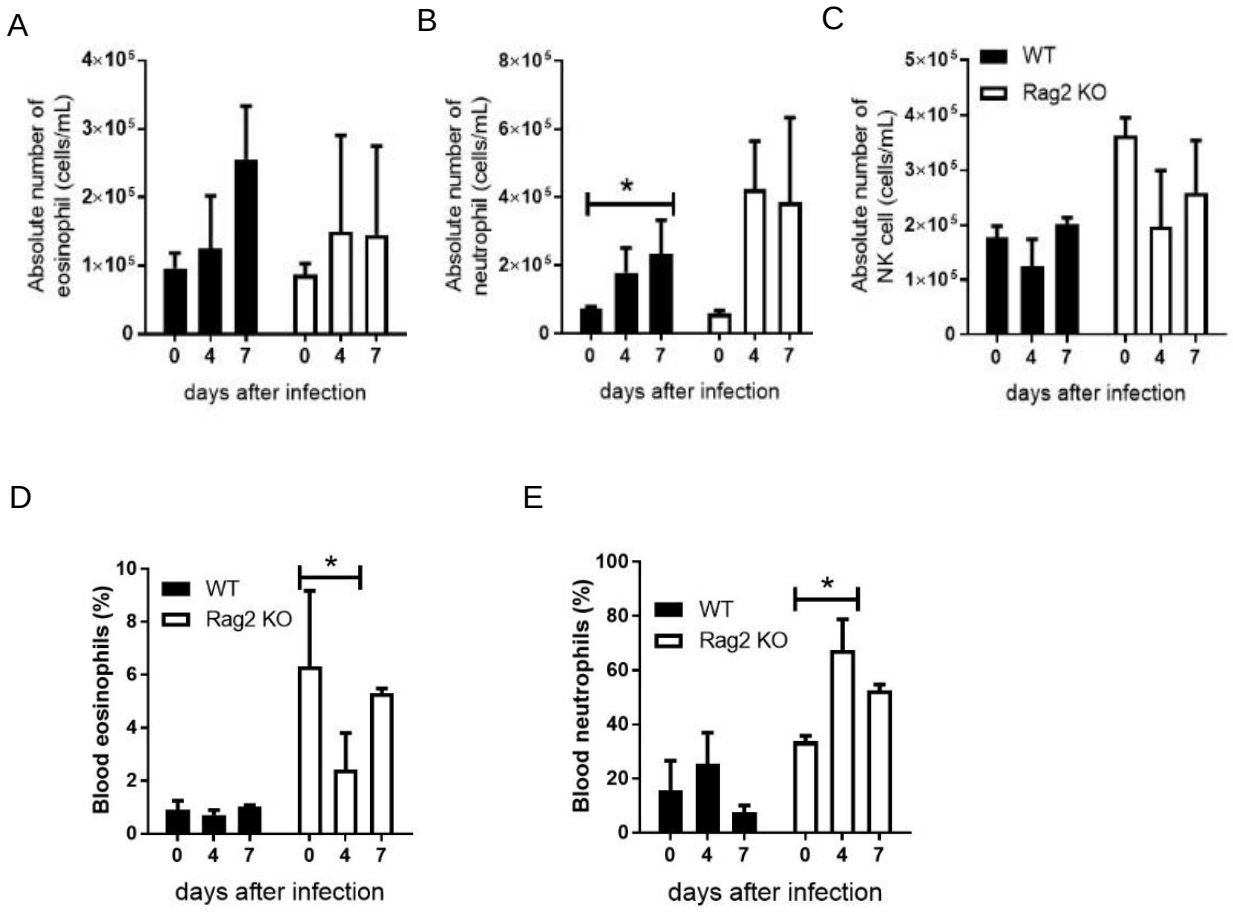

Supplemental figure 3. The kinetics of immune cells in the livers from WT and Rag2 KO mice during ALA formation. Related to Figure 1. The absolute numbers of eosinophil (A; MHC class II$^-$ SiglecF$^+$ CD11b$^+$ cells), neutrophil (B; CD11b$^+$ Gr-1$^+$ F4/80$^-$ MHC class II$^-$ SiglecF$^-$ cells), NK cell (C; CD49b$^+$ NK1.1$^+$ NKp46$^+$ CD3$^-$ MHC class II$^-$ cells), and the proportion of blood eosinophil (D) and neutrophil (E) were analyzed by flow cytometry. Hepatic immune cells and blood cells were isolated from WT and Rag2 KO mice on days 0 (naïve), 4 and 7 after *E. histolytica* injection (n = 3 per time point in each group). Data are representative of three independent experiments with similar results. Statistically significant differences between day 0 and indicated time points in each group are indicated with *P* value (*$P < 0.05$, ANOVA). Each point shows the mean ± standard deviation (SD).

Supplemental figure 4

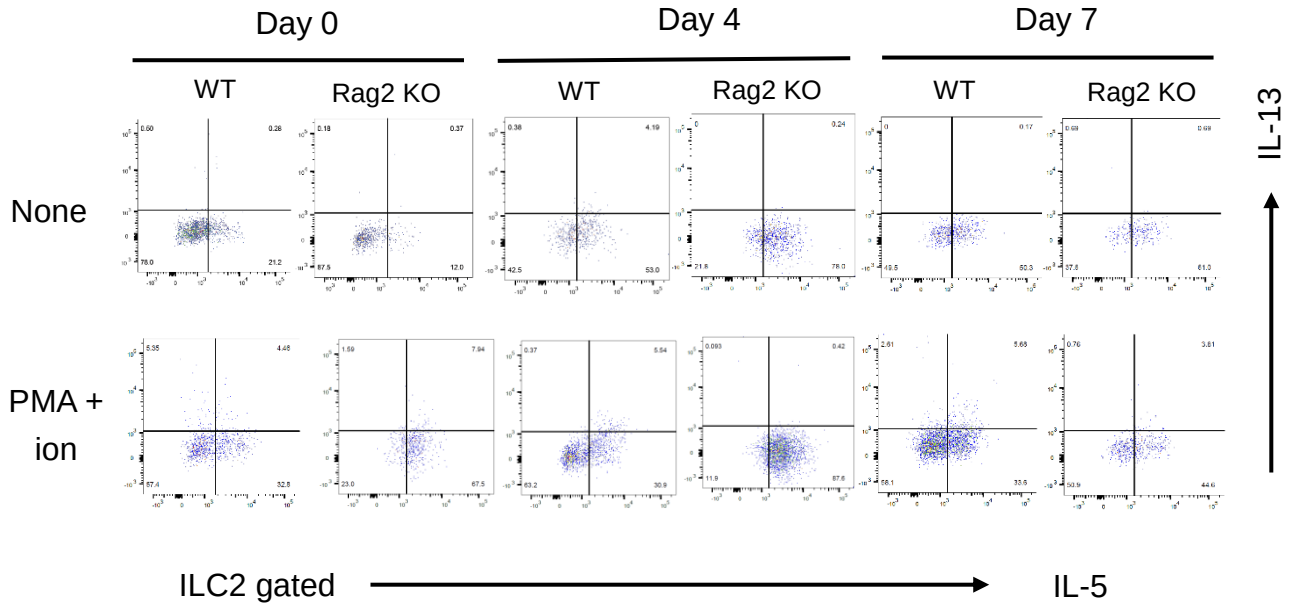

Supplemental figure 4. Dot plots of IL-5$^+$ and IL-13$^+$ ILC2s in the livers from WT and Rag2 KO mice during ALA formation. Related to Figure 2. Flow cytometry of IL-5 and IL-13 producing ILC2s in the livers from WT and Rag2 KO mice on days 0, 4, and 7 (n =3 per each group). The hepatic lymphocytes were stimulated with PMA and ionomycin for 12 hrs. Brefeldin A was added for the last 9 hrs. IL-5 and IL-13-producing ILC2s were detected by intracellular cytokine staining. Representative dot plots were shown after gating ILC2s. Data are representative of three independent experiments with similar results.

Supplemental figure 5

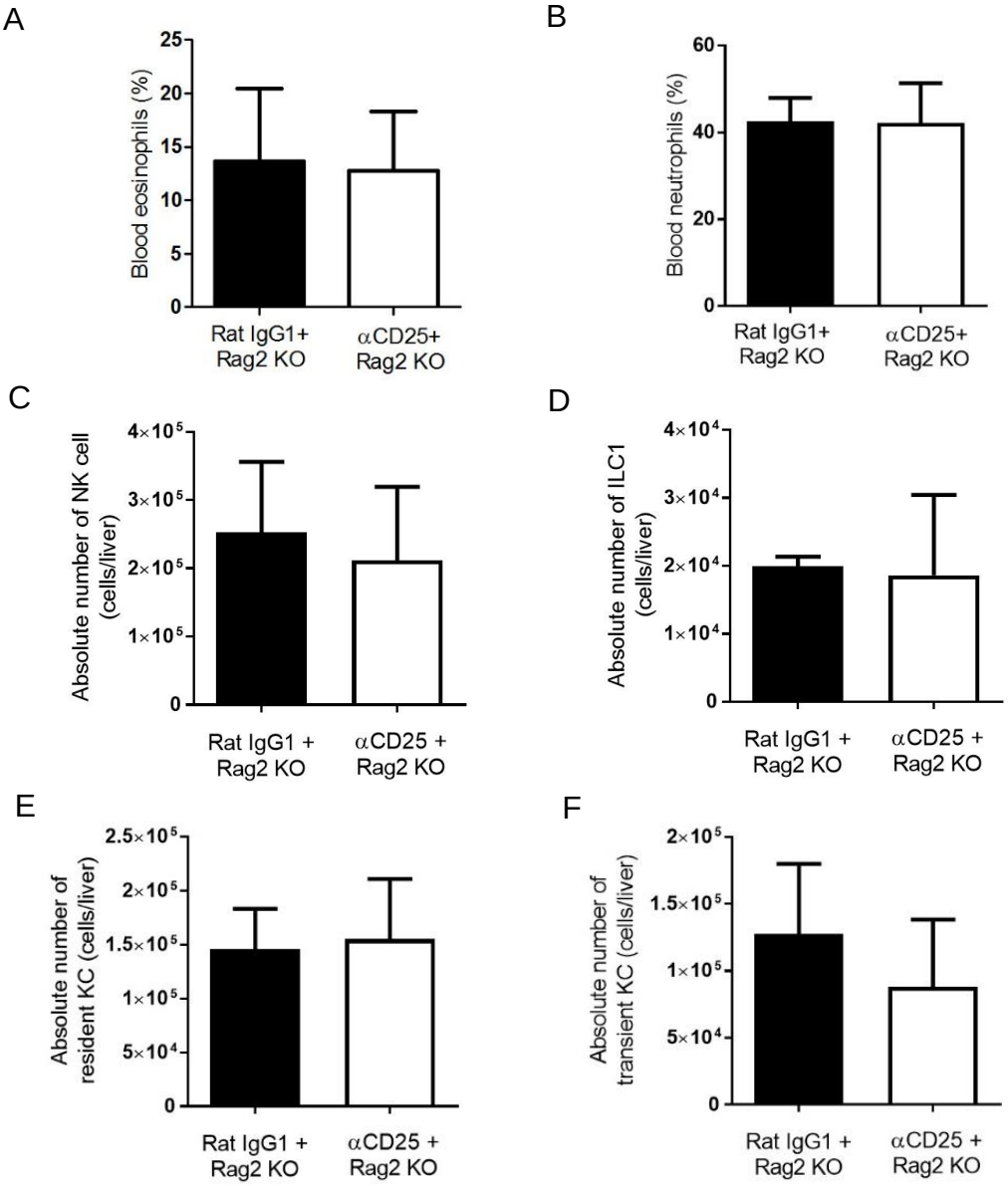

Supplemental figure 5. The effect of αCD25 mAb treatment on other immune cells. Related to Figure 3. (A-F) The proportion of eosinophil (A) and neutrophil (B) in the blood and the absolute numbers of hepatic NK cell (C; KLRG1$^+$ CD49b$^+$ NK1.1$^+$ NKp46$^+$ cells), ILC1 (D; KLRG1$^-$ CD49b$^-$ NK1.1$^+$ NKp46$^+$ cells), resident Kupffer cell (KC) (E; CD11b^{lo} F4/80^{hi} Gr1$^-$ cell) and transient inflammatory monocyte-derived KC (F; CD11b^{hi} F4/80^{lo} Gr1$^-$ cells) were analyzed by flow cytometry. Immune cells in the liver and blood were isolated from Rag2 KO mice treated 2 doses administration of αCD25 mAb (n = 4 in each group). Each data shows the mean ± standard deviation (SD).

Supplemental figure 6

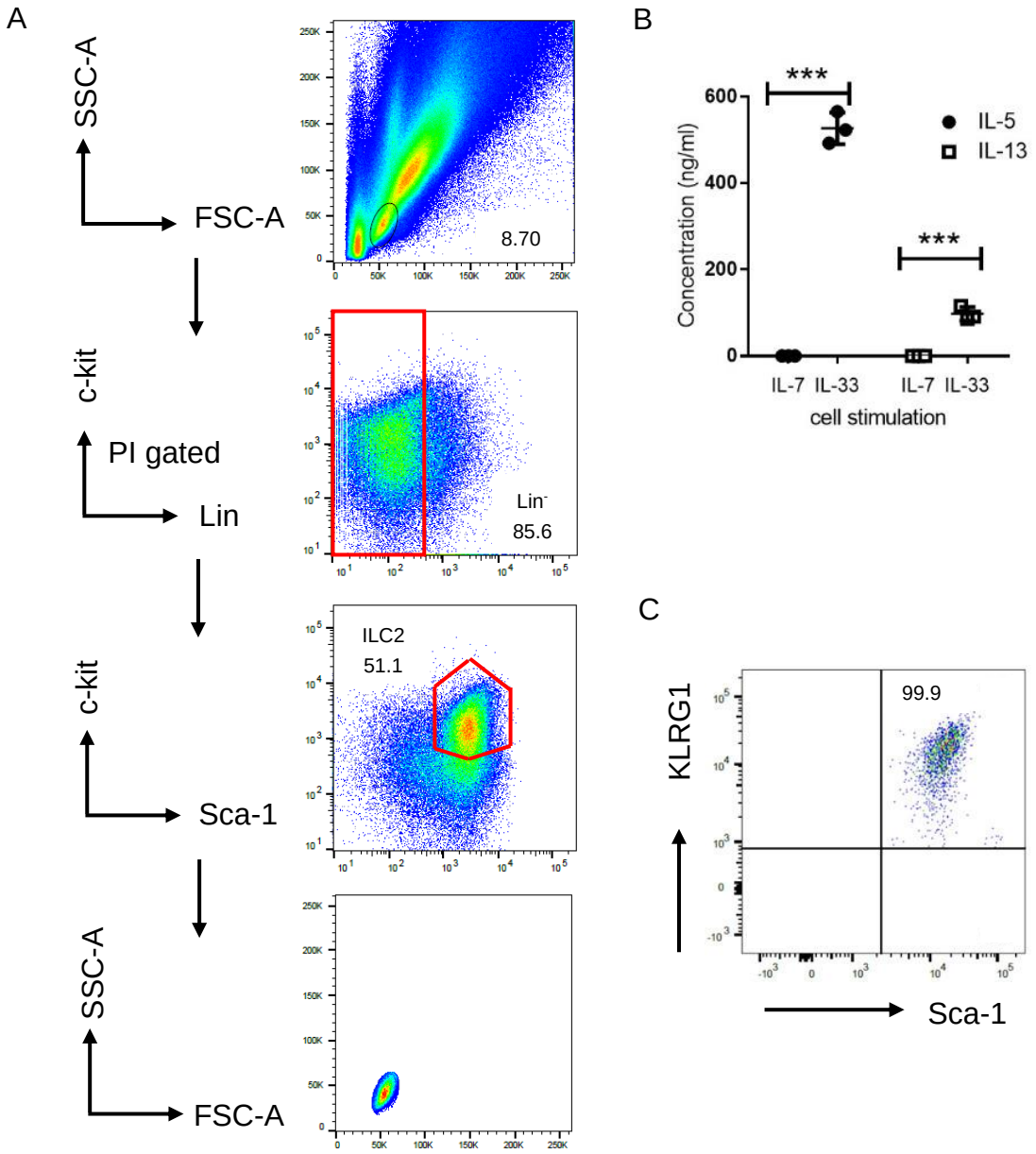

Supplemental figure 6. Sorting strategy and phenotype of transferred ILC2s. Related to Figure 4. The sorting strategy of ILC2s from the mesentery of naïve WT mice by flow cytometry for *in vivo* transfer. Transferred ILC2s were sorted as a c-kit^{+} Sca-1^{+} lineage^{-} PI^{-} cell population (A). IL-5 and IL-13 production by sorted ILC2s co-cultured with IL-33 or IL-7 were measured by Bioplex (B). Statistically significant differences between IL-7 and IL-33 stimulation in each cytokine production are indicated with *P* value (***$P < 0.01$, unpaired *t*-test). Each point shows the mean ± standard deviation (SD). Confirmation of transferred ILC2s presenting in the liver on day 4 after ameba injection by flow cytometry (C; Gata3^{+} CD45^{+} lineage^{-} gated).

Supplemental figure 7

Biotin-conjugated antibodies	Clone
CD11b	M1/70
CD11c	N418
CD3ε	145-2C11
CD19	MB19-1
Ly6G/Ly6C (Gr1)	RB6-8C5
F4/80	BM8
TER-119/Erythroid cells	TER-119
FcεR1α	MAR-1
NK1.1	PK136

Supplemental figure 7. The list of lineage markers for hepatic ILC2 staining. Related to Figure 1 and Transparent Methods. Hepatic lymphocytes were stained for detecting ILC2s with biotin-conjugated antibodies of these lineage markers.

Transparent Methods

Mice. Age- and sex-matched C57BL/6 wild-type (WT) male mice were purchased from Charles River Laboratories Japan (Yokohama, Japan). $Rag2^{-/-}$ (Rag2 KO) mice (Stock #RAGN12), $Rag2^{-/-}\gamma_c{}^{-/-}$ (DKO) mice (Stock #4111) mice were purchased from Taconic. $IL\text{-}33^{GFP/GFP}$ (IL-33-deficient) mice (Oboki et al., 2010) were kindly provided by Dr. Nakae, Hiroshima University. All mice were maintained under specific pathogen-free conditions and offered food and water ad libitum. All mice used were 8-10 weeks old.

Parasite culture and Infection. *E. histolytica* strain JPN51 was kindly gifted from Dr. Eric Houpt, University of Virginia. Trophozoites were serially passaged *in vivo* by intra-cecally inoculating *E. histolytica* to mice, collected from cecal contents and then cultured *in vitro* at 37 °C in Biostate-Iron-Serum-33 (BIS-33) media supplemented with heat-inactivated 10% adult bovine serum, 25 U/ml penicillin and 25 mg/ml streptomycin. An intra-portal vein inoculation procedure was precisely described in a previous publication (Deloer et al., 2016; Goddard et al., 2016). In brief, trophozoites were collected from flasks by cooling them on ice for 3-5 minutes, were then washed by PBS twice. Mice were anesthetized with 1-2% isoflurane (Wako, Tokyo, Japan) using inhalation anesthesia apparatus and were maintained body temperature using the heating pad. Each portal vein

was exteriorized from the peritoneum, and 50 µl of 2 × 10^5 trophozoites were injected into the portal vein ~ 10 mm below the liver at an angle < 5° to the vein, with the bevel facing up. After removed the needle, the injection site was held under pressure with a sterile cotton swab for 3 min. Once mice were stopped bleeding at the injection site of the portal vein, the peritoneal linings and then the skin was sutured with sterile 4-0 vicryl suture and taper needle using a simple continuous or interrupted suture pattern. Uninfected mice were injected 50 µl of PBS into the portal vein in the same way. After the surgical procedure was complete, mice were maintained on a heating pad for recovery in bedding-free, clean cages for a minimum of 20 min.

RNA isolation and quantitative real-time PCR. After sacrifice, 100 µl of liver homogenates were collected and stored at -80°C. Total RNA was extracted using RNeasy Mini Kit (QIAGEN, Hilden, Germany) according to the manufacturer's instructions. The first-stranded cDNA synthesis was done using the PrimeScript RT reagent kit (Takara, Tokyo, Japan) according to the manufacturer's instruction. Real Time-qPCR was performed with QuantiTect® Primer Assay (QIAGEN) for detecting IL-5 (QT00099715), IL-13 (QT00099554), IL-25 (QT00134645) and IL-33 (QT00135170) using QuantiTect® SYBR Green PCR kit (QIAGEN) on the Quant Studio™ 7 Flex Real-Time PCR System

(Applied Biosystems, Life Technologies™, CA, USA). The manufacturer does not open the primer sequences for these cytokines. The cycle time value of each cytokine gene was normalized with GAPDH of the same sample; fold induction for each gene expression was calculated by the ΔCt method. Results obtained each PCR were pooled and statistically analyzed.

Histology and assessment of ALA formation. Liver tissues were removed and fixed in 10% neutral buffered formalin and then embedded in paraffin. After cutting into round slices, the tissue sections were stained with hematoxylin and eosin (H&E) and examined microscopically using NanoZoomer (Hamamatsu Photonics, Shizuoka, Japan). For the assessment of ALA formation, the area and the number of ALA in the liver section of each group of a mouse were calculated by NDP.view 2 software. The area of ALA showed an area of all abscesses in a liver section of each mouse of the group. The number of ALA showed the average of the number of ALA in non-sequential three liver sections from each mouse of the group.

Isolation of hepatic lymphocytes. On indicated days after infection, mice were dissected and hepatic lymphocytes were prepared as described previously (Yajima et al., 2004).

Briefly, liver tissue was removed and separately placed in gentle MACS Octo Dissociator (Miltenyi Biotec, Bergisch Gladbach, Germany) containing 3 ml of HBSS. The resulting homogenate suspension was filtered with 100 μm EASY strainers (Greiner Bio-one, Tokyo, Japan) and pelleted by centrifugation. The pellet was resuspended in RPMI 1640 with 10% FBS containing 33% Percoll (GE Healthcare Bio-Sciences, Uppsala, Sweden) and 10% heparin sodium, then centrifuged at 940 x g for 20 min. Cells at the bottom of the tube were harvested and washed extensively before use.

Antibodies for flow cytometry and immunofluorescence. All cells were stained with various combinations of mAbs. The following mAbs were purchased: biotin-conjugated anti-CD3ε (clone 145-2C11; BioLegend, Tokyo Japan), anti-CD11b (clone M1/70; BioLegend), anti-CD45R/B220 (clone RA3-6B2; BioLegend), anti-I-A/I-E (clone M5/114.15.2; BioLegend), anti-Ly-6G/Ly-6C (Gr-1, clone RB6-8C5; BioLegend), anti-TER-119/ Erythroid Cells (clone TER-119; BioLegend), anti-FcεRIα (clone MAR-1; BioLegend), anti-CD11c (clone N418; Affymetrix, Tokyo, Japan), anti-F4/80 (clone BM8; Affymetrix), anti-CD19 (clone MB19-1; Affymetrix), anti-NK1.1 (CD161, clone PK136; TONBO biosciences, San Diego, CA, USA) and PerCP-Cy5.5 Streptavidin (BioLegend) as the lineage markers (Supplemental figure 7). FITC-conjugated anti-

T1/ST2 (clone DJ8) was purchased from MD Biosciences (Oakdale, MN, USA). PE-conjugated anti-GATA3 (clone L50-823), anti-SiglecF (clone E13-161.7), anti-KLRG1 (clone 2F1), PE-Cy7-conjugated anti-CD127 (clone SB/199), anti-CD117 (c-kit, clone 2B8) and FITC-conjugated anti-NKp46 (CD335, clone 29A1.4), anti-Ly-6A/E (Sca-1, clone E13-161.7) were purchased from BD Biosciences (San Jose, CA, USA). Allophycocyanin (APC)-conjugated anti-CD127 (clone SB/199), anti-IL-5 (clone-TRFK5), anti-CD49b (clone Dx5), anti-IL-17RB (clone 9B10), APC-Cy7-conjugated anti-CD25 (clone PC61), anti-CD45 (clone 30-F11), FITC-conjugated anti-CD11b (clone M1/70), anti-NK1.1 (clone PK136), PE-conjugated anti-Ly-6G/Ly-6C (Gr-1, clone RB6-8C5) and PE-Cy7-conjugated anti-Thy1.2 (CD90.2 clone 30-H12), anti-CD45 (clone 30F11), anti-F4/80 (clone BM8) were purchased from BioLegend. PE-Cy7-conjugated anti-IL-13 (clone eBio13A) and PE-conjugated anti-IL-5 (clone TRFK5) were purchased from Affymetrix. The stained cells were acquired and analyzed in a FACSVerse flow cytometer (BD Biosciences). The data were analyzed using FlowJo v10 software (FlowJo, LLC, Ashland, OR, USA). The following anti-mouse antibodies used for immunofluorescence: anti-mouse IL-33 antibody (Catalog # AF3626; R&D Systems), Alexa Fluor® 647-conjugated anti-GATA3 (Clone L50-823, Catalog # 560078; BD Pharmingen^{TM}), PE-conjugated anti-IL-33 receptor (T1/ST2) (Clone U29-93 Catalog #

566311; BD Pharmingen™), Alexa Fluor® 488-conjugated donkey anti-goat IgG (H+L) (Catalog # A11055; Thermo Fisher Scientific), Alexa Fluor® 555-conjugated donkey anti-rabbit IgG (H+L) (Catalog # A31572; Thermo Fisher Scientific), anti-phycoerythrin antibody (Catalog # PA5-35006; Thermo Fisher Scientific) and anti-mouse CD16/32 (Fc Block, clone 2.4G2; purified in our lab).

Intracellular cytokine staining. Hepatic lymphocytes were incubated without any stimulation or with 20 ng/ml PMA (Sigma) and 1 μg/ml ionomycin (Invitrogen) for 12 h at 37°C in 5% CO_2, and 10 μg/ml brefeldin A (Sigma-Aldrich) added 3 h later, at a concentration of 1×10^6 in RPMI containing 10% FCS. After culture, cells were stained with various combinations of mAbs. After surface staining, cells were subjected to staining of intracellular-cytokine and transcription factor using the manufacturer's instructions. In brief, for transcription factor staining, 1 ml of fix and permeabilization solution (Foxp3 transcription staining kit, eBiosciences) was added to the cell suspension with mild mixing and placed for 20 min at RT. Fixed cells were washed with 2 ml of Perm/Wash solution (eBiosciences) twice and were stained intracellularly with various combinations of antibodies for 30 min at RT. For intracellular cytokine staining, cells were fix and permeabilization with IntraPrep Permeabilization Reagent (Beckman

Coulter, Brea, CA, US). Samples were acquired in a FACSVerse flow cytometer (Becton, Dickinson, Franklin Lakes, NJ, US) and analyzed by FlowJo V10 software.

ELISA and Bioplex. Supernatants of the liver homogenates from mice at the indicated times after *E. histolytica* injection were obtained by centrifugation at 440 × g for 3 min at 4 °C. For the detection of IFN-γ in the culture supernatants of the hepatic lymphocytes, 5 × 10^5 cells/ well of whole hepatic lymphocytes were stimulated with PMA (20 ng/ml) and ionomycin (1 μg/ml) for 3 days, then IFN-γ secretion in the supernatants were measured with a DuoSet ELISA development system (DY485, R&D Systems) according to the manufacturer's instructions. Briefly, 96-well immune plates were coated with a goat-anti-mouse IFN-γ affinity-purified antibody (Ab) as the capture Ab. Following primary incubation, samples were treated with biotinylated goat anti-mouse IFN-γ mAb to detect these cytokines. Plates were subsequently incubated with streptavidin conjugated to HRP and visualized using a substrate solution. For the measurement of IL-5 and IL-13 by Bioplex, 1 × 10^4 of sorted mesentery ILC2s were co-cultured with IL-7 or IL-33 (10 ng/ml) for 5 days. Then, IL-5 and IL-13 secretion in the supernatants were measured with Bio-Plex Pro mouse cytokine GI 23-Plex (Panel #M60009RDPD, Bio-Rad) according to the manufacturer's instructions and detected by Bioplex 200 (Bio-Rad). The data were

analyzed by Bio-Plex Manager Software.

***In vivo* depletion of ILC2s and neutralization of IL-5.** To deplete ILC2s, anti-mouse (α) CD25 (IL-2Rα) mAb (clone PC-61.5.3; BioXCell, West Lebanon, NH, USA) was intraperitoneally injected into Rag2 KO mice at a dose of 200 μg/ mouse every 2 days from 3 days before *E. histolytica* infection. The isotype-matched control IgG (Rat IgG1, clone HRPN) was obtained by BioXCell. For the confirmation of ILC2-depletion, hepatic lymphocytes from the mice administrated αCD25 mAb was purified and analyzed a proportion of lineage$^-$ CD45$^+$ Gata3$^+$ Thy1.2$^+$ T1/ST2$^+$ ILC2s using flow cytometer. To neutralize IL-5, αIL-5 mAb (clone TRFK5; BioXCell) was intraperitoneally injected into Rag2 KO mice at a dose of 250 μg/ mouse every 2 days from 3 days before *E. histolytica* infection. Rat IgG1 for αCD25 mAb (clone HRPN) was used as the isotype-matched control IgG for αIL-5 mAb.

Adoptive transfer of ILC2s. Naïve ILC2s were isolated from the mesentery of WT mice as described (Moro et al., 2015) and cultured in 96-well round bottom plate with RPMI-1640 medium (Sigma) containing 10% FCS, 50 μM 2-mercaptoethanol (Gibco), 100 U/ml penicillin and 100 μg/ml streptomycin (Gibco), 1× non-essential amino acids

(Sigma), 10 mM HEPES (Sigma), and 1 mM sodium pyruvate (Gibco) and IL-2 (10 ng/ml) (Moro et al., 2015). A total of 2×10^6 cultured naïve ILC2s were intravenously transferred into the naïve Rag2$^{-/-}\gamma_c^{-/-}$ double KO mice one day before *E. histolytica* injection.

Immunofluorescence.

Infected or uninfected liver tissues were harvested, submerged into 20% sucrose overnight and embedded into O.C.T compound (Sakura Finetek U.S.A., Inc., Torrance, CA) to be snap frozen using liquid nitrogen. Sectioning was performed on a cryostat (Leica CM 1950) at 3.5μm thickness. Thoroughly air-dried sections were fixed with ice-cold acetone/methanol (1:1 mixture) for 5 min, air-dried again, and stored, if needed, in -80 °C until use. After being rehydrated with PBS for 5 min sections were blocked with 5% FBS in PBS-T (0.05% Tween) and Fc Block (5 μg/mL) in a moisture box for 2h at room temperature. Sections were stained with anti-mouse IL-33 antibody (1:50 dilution, 1% FBS in PBS-T), PE-conjugated anti-IL-33 receptor (T1/ST2) (1:200) and Alexa Fluor® 647-conjugated anti-GATA3 (1:50) overnight at 4 °C. Slides were rinsed with PBS-T on a shaker for 30 min at 4 °C. To amplify PE-conjugated antibody for primary staining, sections were labeled with rabbit anti-phycoerythrin antibody (1:400) for 1h at

4 °C, washed for 30 min again, further incubated with Alexa Fluor® 555-conjugated donkey anti-rabbit IgG (H+L) antibody (1:1600) for 1h at 4 °C as previously described (Yoshizawa et al., 2018). To visualize non-labeled purified antibody for primary staining, like anti-IL-33, Alexa Fluor® 488-conjugated donkey anti-goat IgG (H+L) (1:800) was used for secondary antibody simultaneously. After final wash for 30 min, sections were mounted with ProLong™ Diamond Antifade with DAPI (Thermo Fisher Scientific). Leica TCS SP8 laser scanning confocal microscope equipped with an acousto-optical beam splitter (AOBS) system (Leica Camera AG, Wetzlar, Germany) with a 40x oil objective (PL APO, NA1.25) was also used for image acquisition with LAS AF software. Image processing and analyses were carried out using for Fiji/ImageJ (http://rsbweb.nih.gov/ij/) as well.

Statistics. Figures and Statistical significance were evaluated GraphPad Prism software (GraphPad, San Diego, CA, USA). Mice were allocated to experimental groups based on their genotypes and treatments. There is no mouse to exclude from the analyses. For assessments of ALA and analyses of hepatic lymphocytes infiltration, unpaired 2-tailed Student's t-test was performed when 2 experimental groups were compared. For the kinetics of lymphocyte number and mRNA expression compared with day 0 in each group

and *in vivo* transfer experiment, 1-way ANOVA was performed. *P* values with <0.05 were considered to represent a significant difference.

Study approval. This study was approved by the Committee of Ethics on Animal Experiments of the Nagasaki University (the approval number of animal experiments; 1502181226, the approval number of recombinant DNA experiments; 1902201550) and RIKEN. Experiments were carried out under the control of the Guidelines for Animal Experiments of both Nagasaki University and RIKEN.

Supplemental References

DELOER, S., NAKAMURA, R., MI-ICHI, F., ADACHI, K., KOBAYASHI, S. & HAMANO, S. 2016. Mouse models of amoebiasis and culture methods of amoeba. *Parasitol Int,* 65**,** 520-525.

GODDARD, E. T., FISCHER, J. & SCHEDIN, P. 2016. A Portal Vein Injection Model to Study Liver Metastasis of Breast Cancer. *J Vis Exp*.

MORO, K., EALEY, K. N., KABATA, H. & KOYASU, S. 2015. Isolation and analysis of group 2 innate lymphoid cells in mice. *Nat Protoc,* 10**,** 792-806.

OBOKI, K., OHNO, T., KAJIWARA, N., ARAE, K., MORITA, H., ISHII, A., NAMBU, A., ABE, T., KIYONARI, H., MATSUMOTO, K., SUDO, K., OKUMURA, K., SAITO, H. & NAKAE, S. 2010. IL-33 is a crucial amplifier of innate rather than acquired immunity. *Proc Natl Acad Sci U S A,* 107**,** 18581-6.

YAJIMA, T., NISHIMURA, H., SAITO, K., KUWANO, H. & YOSHIKAI, Y. 2004. Overexpression of Interleukin-15 increases susceptibility to lipopolysaccharide-induced liver injury in mice primed with Mycobacterium bovis bacillus Calmette-Guerin. *Infect Immun,* 72**,** 3855-62.

YOSHIZAWA, A., BI, K., KESKIN, D. B., ZHANG, G., REINHOLD, B. & REINHERZ, E. L. 2018. TCR-pMHC encounter differentially regulates transcriptomes of tissue-

resident CD8 T cells. *Eur J Immunol,* 48**,** 128-150.